Available online at www.sciencedirect.com
ScienceDirect
Remote Sensing of Environment 107 (2007) 120–137
Remote Sensing of Environment
www.elsevier.com/locate/rse

Simultaneous retrieval of aerosol and surface optical properties using data of the Multi-angle Imaging SpectroRadiometer (MISR)

Johannes Keller [a,*], Stephan Bojinski [b], André S.H. Prevot [a]

[a] Paul Scherrer Institute, Laboratory of Atmospheric Chemistry (LAC), CH-5232 Villigen PSI, Switzerland
[b] World Meteorological Organization (WMO), Global Climate Observing System Secretariat (GCOS), 7bis, Avenue de la Paix, Case Postale 2300, CH-1211 Geneva 2, Switzerland

Received 28 February 2006; received in revised form 20 June 2006; accepted 31 July 2006

Abstract

An algorithm for retrieving simultaneously aerosol and surface optical properties from radiance data of the Multi-angle Imaging SpectroRadiometer (MISR) was developed. It uses MISR subregion radiance data of the 9 cameras and 4 spectral bands (spatial resolution 1.1 km) to generate characteristic functions $\rho_{surf}=f_{\lambda,cam}$ (β_e (550 nm)), where β_e (550 nm) and ρ_{surf} are the ground level aerosol extinction coefficient at 550 nm, and the surface reflectance, respectively. The analysis of the mutual intersections of those functions yield optimum values for β_e (550 nm), aerosol optical depth (AOD) at 550 nm and ρ_{surf}. MODTRAN 4 v3r1 was used to create radiance look-up tables. The algorithm was tested for MISR paths covering the complex terrain of Switzerland and northern Italy. Results of 2 days (low and high aerosol loads on May 14 and June 17, 2002, respectively) were analyzed and compared with sun photometer measurements. First, ground level aerosol extinction coefficients and optical depth over water were derived. From those data it was possible to retrieve a best-fit aerosol mixture. AOD (550 nm) over water is in satisfactory agreement with both sun photometer data and the operational aerosol product of MISR. Second, the Ross–Li approach for the bidirectional reflectance factor (BRF), supported by MODTRAN 4, was applied to simulate the radiance over vegetation surfaces. In this case, the retrieved aerosol extinction coefficients and optical depths over vegetation are significantly lower than the values derived over water. We assume that the incomplete coupling of BRF and radiation in MODTRAN 4 is at least partly responsible for this discrepancy.

Keywords: MISR; MODTRAN 4; Aerosols; Aerosol optical depth; Surface reflectance

1. Introduction

Aerosols affect mankind mainly in two ways. First, they modify the radiation balance of the earth in a direct (increased backscattering of solar radiation to space) and in an indirect way (cloud formation activated by particulates). These effects may significantly contribute to climate change. The radiative forcing of these contributions, however, is still fraught with high uncertainties (Houghton et al., 2001). Second, epidemiological studies showed that respiratory symptoms, lung function and mortality are significantly correlated with the mass density of the particulate matter below 10 μm (Dockery et al., 1993; Fischer et al., 2004; Stedman, 2004). Hence it is desirable to obtain information on aerosol properties both globally as well as on a local or regional scale.

Satellite sensors have the potential of measuring the spatial and temporal distribution of aerosol properties from space. The retrieval of these properties is based on the measurement of scattered sunlight. The angular pattern and the wavelength dependence of the scattered radiation strongly depend on characteristic quantities of aerosols such as particle size distribution, single scattering albedo, non-sphericity and refractive index. The radiance measured by downward looking remote sensing instruments is a mixture of scattered and reflected radiation. A review of approaches to derive aerosol optical properties is given by King et al. (1999).

During the last few years, novel instruments have been developed and launched. Multi-angle viewing sensors are particularly suited for the retrieval of aerosol optical properties. Along-track angular variations of radiance measurements, for

* Corresponding author. Tel.: +41 56 3102065; fax: +41 56 3104525.
E-mail address: johannes.keller@psi.ch (J. Keller).

0034-4257/$ - see front matter © 2006 Elsevier Inc. All rights reserved.
doi:10.1016/j.rse.2006.07.020

instance, may be exploited to retrieve the scattering phase function. The most powerful instrument for multi-angular observations currently in orbit is the Multi-angle Imaging SpectroRadiometer (MISR) aboard Terra (Diner et al., 1998). MISR observes the earth at 9 different view angles and 4 spectral bands at a pixel resolution of 275 m and averages the radiance data onboard over subregions of 1.1 km. An operational aerosol product from MISR is available at a 17.6 km resolution. This resolution, however, is too coarse to be meaningful for complex topography such as Switzerland. Hence, we developed a novel retrieval algorithm that yields information on both surface reflectance and aerosol optical properties on the subregion resolution. Details about MISR and its use for the operational retrieval of aerosol properties are given in Section 2. Section 3 describes the retrieval algorithm. Finally, Section 4 reports the application of the algorithm and the results for low and high aerosol load in Switzerland and the Po Basin in northern Italy.

2. MISR instrument and aerosol related data products

The Multi-angle Imaging SpectroRadiometer (MISR) onboard the NASA Terra satellite has 9 pushbroom cameras (An, Af, Aa, Bf, Ba, Cf, Ca, Df, Da) pointing at 9 different view angles. They look at nadir (n), forward (f), and afterward (a) directions (nominal zenith angles: 0, 26.1, 45.6, 60.0 and 70.5^0). Each camera has 4 spectral bands (blue: 446 nm, green: 557 nm, red: 672 nm and near infrared (NIR): 866 nm). A detailed description of the instrument is available from Diner et al. (1998). The Level 1B2 product includes calibrated top of atmosphere (TOA) radiances geo-rectified either on the World Geodetic System 1984 (WGS84) ellipsoid or on the terrain. Radiance measurements are taken at a pixel resolution of 275 m and averaged onboard over subregions of 1.1 km before being transmitted to ground. Data of the nadir camera An (all bands) and of the red band (all cameras) are transmitted at the pixel resolution. On request, local mode data are taken with 275 m resolution for all bands and cameras. Geometric parameters such as altitude, solar and view angles for each subregion may be extracted from the data sets for further processing.

Terra follows 233 paths covering the entire globe. The satellite revisits the same path every 16 days. Due to the MISR swath width of 380 km, the effective repetition period for a given ground location varies between 2 and 7 days. The data of one semi-orbit is split into 180 blocks. Blocks 52 to 54 of paths 193 to 197 cover Switzerland.

An operational aerosol product is available on regional grids with a resolution of 17.6 km × 17.6 km. The product is calculated with an algorithm developed by Martonchik et al. (1998). This product is based on a set of climatological aerosol mixtures. Each of them consists of 3 components (called aerosol models) selected from a number of possible aerosols. These mixtures are supposed to cover the most likely maritime, rural and urban conditions. Phase functions for each component are included as well. Since the launch of MISR, the composition of aerosol mixtures has been modified at least twice. The most recent version is V3.3 (January 2006). For the investigation described in this publication, version V2.2 was used (see Tables 1 and 2). Pre-calculated radiances are compared with the measured values of each camera and wavelength. The output contains, among other quantities, the regional mean (or best estimate) AOD in the green band and the corresponding mixture. Aerosol properties are computed for both water and land surfaces. Cloudy and mountainous areas are masked out.

A research version of the aerosol algorithm software is currently being developed for non-operational use that is

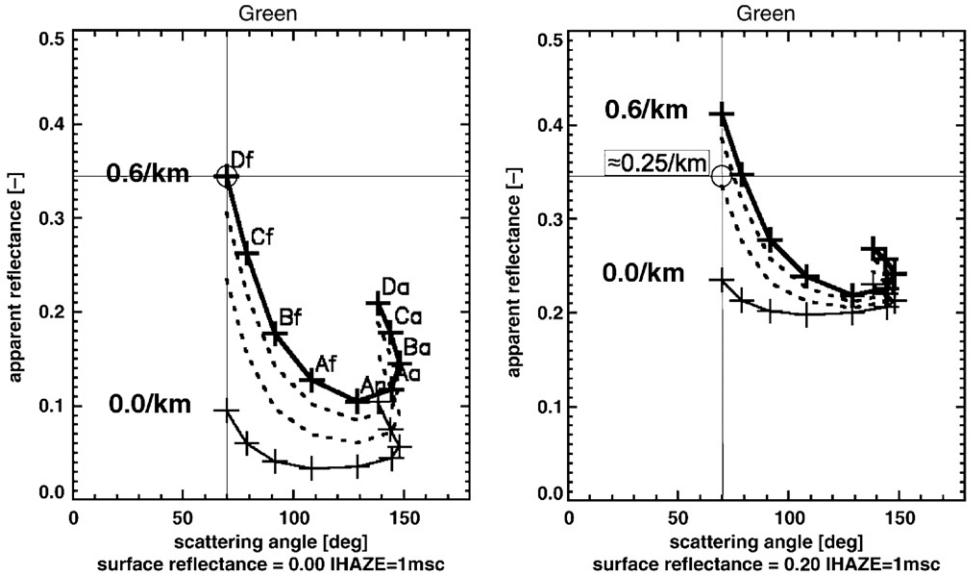

Fig. 1. Simulated apparent reflectance ρ_{app} measured by the 9 MISR cameras vs. scattering angle for the green spectral band (557 nm). Af to Df: forward looking cameras, Aa to Da: aftward looking cameras, An: nadir looking camera. Ground level extinction coefficients β_e (550 nm) are set to 0 (thin solid line), 0.2, 0.4 (dotted lines, not labeled) and 0.6 km^{-1} (thick solid). Surface reflectances ρ_{surf} are set to 0 (left panel) and 0.2 (right panel). The surface is assumed to be Lambertian. Example: $\rho_{app}=0.345$ is observed by camera Df (crosshair) for $\rho_{surf}=0.0$ and β_e (550 nm) = 0.6 km^{-1} (left) as well as for $\rho_{surf}=0.2$ and β_e (550 nm) = 0.25 km^{-1} (right). See text for details.

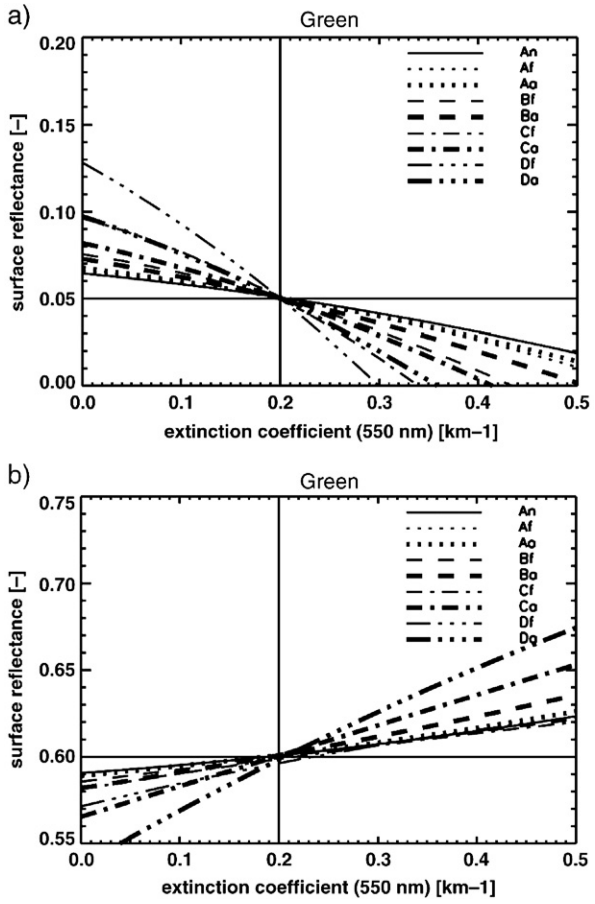

Fig. 2. Simulated surface reflectance ρ_{surf} vs. ground level aerosol extinction coefficient β_e (550 nm) for the MISR cameras Df to Da. The top of atmosphere (TOA) radiance L (λ,cam) of each camera is kept constant for the full range of β_e (550 nm) and corresponds to the radiance L_{ref} (λ,cam) of the green band at the reference values $\beta_{e,ref}$ (550 nm)=0.2 km^{-1} and $\rho_{surf,ref}$. a): dark surface ($\rho_{surf,ref}$=0.05), b): bright surface ($\rho_{surf,ref}$=0.60). See text for details.

capable of calculating aerosol properties on a subgrid resolution. However, it is applicable only for a small number of subregions (Kahn, 2006).

All MISR products together with numerous ancillary data are available online from the Earth Observing System (EOS) Data Gateway (EOSDIS, 2001) or from the MISR Order and Customization Tool provided by the NASA Langley Atmospheric Sciences Data Center (NASA_Langley_ASDC, 2006).

3. Simultaneous Retrieval (SR) method

3.1. Radiative transfer model

The radiative transfer model (RTM) we used for the forward simulations of radiances and transmittances is the widely used MODTRAN 4 code (Acharya et al., 1999; Berk et al., 2003, 1999). The current release is v3r1. Input data may be explicitly specified, e.g. vertical profiles of meteorological parameters and atmospheric constituents, optical properties of aerosols). The basic optical quantity used as input is the extinction coefficient β_e (550 nm). Wavelength dependent extinction and absorption coefficients are specified relative to that value. MODTRAN 4 supports the DISORT N-stream option for multiple scattering in inhomogeneous atmospheres. Optical properties of the ground surface may be specified either as Lambertian or by Bidirectional Reflectance Distribution Functions (BRDFs).

In an inter-comparison workshop in the framework of ACCENT/TROPOSAT 2 (Wagner et al., in press) 10 RTMs based on different algorithms were tested for various geometries and vertical atmospheric profiles. Since the workshop was focused on Multi-Axes Differential Absorption Spectroscopy (MAXDOAS), only upward looking view paths were included. The MODTRAN 4 radiances show a close match to the results of the other models. Hence, we are confident that MODTRAN 4 correctly models scattering and absorption of radiation by gaseous and particulate constituents of the atmosphere. Radiance inter-comparisons for downward looking geometries including various surface types are yet to be considered.

3.2. Retrieval algorithm

3.2.1. Principle

Let us assume an idealized atmosphere with given trace gas and aerosol compositions and profiles located at northern mid-latitude. The tropospheric aerosol column density of this atmosphere is variable. It is controlled by the aerosol extinction coefficient β_e (550 nm) at ground level. In the simplest case the ground surface is a Lambertian reflector with variable reflectance ρ_{surf}. Fig. 1 shows a typical relationship of the apparent reflectance ρ_{app} vs. the scattering angle of the camera Df to Da for β_e (550 nm)=0.0 (thin solid), 0.2, 0.4 (dotted) and 0.6 km^{-1} (thick solid), and ρ_{surf}=0.0 (left panel) and 0.2 (right panel). The apparent reflectance is defined as $\rho_{app}=\pi L$ (λ,cam)/(E_0 cosθ_s), where L (λ,cam) is the TOA radiance in the spectral band λ for the view geometry of camera cam. E_0 is the extraterrestrial irradiance and θ_s is the solar zenith angle. It is evident from Fig. 1 that in the case of a substantial aerosol load the cameras looking forward at large zenith angles (e.g. Df) observe the same location as an apparently brighter target than the corresponding aftward looking sensors (e.g. Da). At low surface reflectance (e.g. ρ_{surf}=0.0),

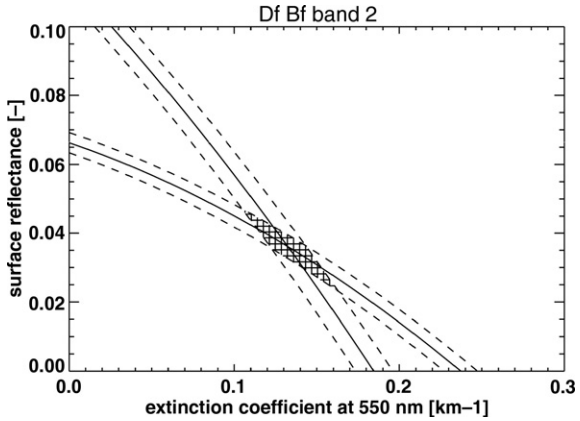

Fig. 3. Example of the uncertainties of the extinction coefficient β_e (550 nm) and the surface reflectance ρ_{surf} (hatched area) retrieved from the intersections of the characteristic functions of the cameras Df and Bf. See text for details.

Table 1
Basic aerosol models used in the MISR Aerosol Climatology Product

Model	Description	r_{eff} [μm]	r_{min} [μm]	r_{max} [μm]	h_s [km]	ω_0 [−]
1	Spherical, non-absorbing (sulfate, sea salt, organic)	0.0562	0.001	0.4	2	1.0
2	Spherical, non-absorbing (sulfate, sea salt, organic)	0.1212	0.001	0.75	2	1.0
3	Spherical, non-absorbing (sulfate, sea salt, organic)	0.2620	0.01	1.5	2	1.0
4	Spherical, non-absorbing (sulfate, sea salt, organic)	0.5687	0.01	4.0	2	1.0
5	Spherical, non-absorbing (sea salt, organic)	1.2835	0.01	8.0	2	1.0
6	Spherical, non-absorbing (water soluble)	6.9557	0.1	50.0	2	1.0
7	Non-spherical, absorbing (red dust)	1.1755	0.05	2.0	2	0.88
8	Non-spherical, absorbing (red dust)	1.1755	0.05	2.0	10	0.88
9	Non-spherical, absorbing (red dust)	7.4849	0.5	15.0	10	0.69
10	Spherical, absorbing (black carbon)	0.0399	0.001	0.5	10	0.21
11	Non-spherical, non-absorbing (thin cirrus)	21.56	3.0	200.0	10	1.0

r_{eff}: effective radius, r_{min}: minimum radius, r_{max}: maximum radius, h_s: layer scale height, ω_0: single scattering albedo.

enhanced aerosol loads brighten the target. For bright surfaces (not shown in Fig. 1) the observed radiance decreases due to extinction of the reflected radiation (see also King et al. (1999)).

For β_e (550 nm)=0.6 km^{-1} and ρ_{surf}=0.0 (left panel of Fig. 1), the apparent reflectance observed by camera Df in the green band is about 0.345 (see crosshair). The simulation yields the same radiance, i.e. the same apparent reflectance, also for other input data pairs [β_e (550 nm), ρ_{surf}], e.g. β_e (550 nm)≈0.25 km^{-1} and ρ_{surf}=0.2 (right panel). In other words, over dark targets a small increase of the surface reflectance must be compensated by decreased aerosol scattering to keep the apparent reflectance constant. Hence it is possible to generate functions $\rho_{surf}=f_{\lambda,cam}$ (β_e (550 nm)). These functions are determined by the camera and wavelength dependent radiance L (λ,cam)=L_{ref} (λ,cam) simulated for specified reference values $\beta_{e,ref}$ (550 nm) and $\rho_{surf,ref}$.

As an example, Fig. 2a shows these functions for each camera, the green spectral band, and the respective radiances simulated for the reference values $\beta_{e,ref}$ (550 nm)=0.2 km^{-1} and $\rho_{surf,ref}$=0.05. The correlations are nearly linear and obviously have a common intersection at β_e (550 nm)=$\beta_{e,ref}$ (550 nm)= 0.2 km^{-1} and $\rho_{surf}=\rho_{surf,ref}$=0.05. All slopes are negative, which indicates the brightening of the observed target due to aerosol backscattering. This means that the surface reflectance must decrease for an increasing aerosol extinction coefficient (increasing backscattering) in order to keep the TOA radiance L (λ,cam)=L_{ref} (λ,cam) constant. Bright surfaces such as sand (e.g. ρ_{surf}=0.6) cause negative slopes due to extinction of the enhanced reflected radiation (Fig. 2b).

As mentioned above, the functions and their common intersections shown in Fig. 2 were generated by starting with known values of $\beta_{e,ref}$ (550 nm) and $\rho_{surf,ref}$ used as input to simulate the unknown radiance L (λ,cam). In reality, however, L (λ,cam) is known from the measurements L_{MISR} (λ,cam) taken by MISR, and β_e (550 nm) and ρ_{surf} are the unknowns to be determined.

This inverse procedure consists of the following basic steps:

a) Look-up tables (LUTs) of the radiance, L_{LUT} (λ,cam), for each camera cam and spectral band (central wavelength λ) are calculated for specified aerosol compositions, profiles, topographic heights, and for geometries valid for the MISR scenes of interest. These LUTs contain TOA radiances for a set of ground level extinction coefficients $\beta_{e,LUT}$ (550 nm) (currently 0.0, 0.2, 0.5 and 0.8 km^{-1}) and surface reflectance values $\rho_{surf,LUT}$ (currently 0.0, 0.05, 0.2 and 0.6). Additional simulations for the set of $\beta_{e,LUT}$ (550 nm) yield LUTs of the vertical transmittance and aerosol optical depth (AOD).
b) The surface reflectance ρ_{surf} expected for the set of $\beta_{e,LUT}$ (550 nm) and for L_{MISR} (λ,cam) is evaluated by interpolating the radiance LUT for L_{MISR} (λ,cam). The relationship $\rho_{surf}=f_{\lambda,cam}$ (β_e (550 nm)), denoted as "characteristic function", is finally obtained by approximating the 4 data points by a suitable analytical function, e.g. a 2nd order polynomial.
c) Provided the atmospheric conditions (except β_e (550 nm)) at the time of overpass are exactly the same as those supposed by the RTM, the characteristic functions of all cameras are similar to those of Fig. 2. The intersections, denoted by the subscript "in", of the functions belonging to the cameras cam i and cam k, [$\beta_{e,in}$ (550 nm), $\rho_{surf,in}$]=[$\beta_{e,cam\ i,\ cam\ k}$ (550 nm), $\rho_{surf,cam\ i,cam\ k}$], calculated for all cameras, coincide at one single point and yield simultaneously the extinction coefficient at 550 nm and the surface reflectance. It is worth mentioning that if the atmosphere were known as assumed above, only 2 cameras would be needed to retrieve [$\beta_{e,in}$ (550 nm), $\rho_{surf,in}$].
d) Finally, the AOD LUT is interpolated taking the retrieved $\beta_{e,in}$ (550 nm) as input.

Table 2
Aerosol mixtures of the MISR Aerosol Climatology Product V2.2 used in this study

Mixture	Model 1 (fraction)	Model 2 (fraction)	Model 3 (fraction)
1	1 (1.0)	2 (0.0)	3 (0.0)
3	1 (0.0)	2 (1.0)	3 (0.0)
5	3 (1.0)	4 (0.0)	5 (0.0)
7	3 (0.0)	4 (1.0)	5 (0.0)
8	3 (0.0)	4 (0.5)	5 (0.5)
9	1 (0.0)	2 (0.5)	5 (0.5)
10	1 (0.5)	2 (0.0)	5 (0.5)
11	1 (0.85)	2 (0.0)	10 (0.15)
12	1 (0.45)	2 (0.4)	10 (0.15)
13	1 (0.0)	2 (0.85)	10 (0.15)
15	3 (0.85)	4 (0.0)	10 (0.15)
17	3 (0.0)	4 (0.85)	10 (0.15)
18	3 (0.75)	7 (0.25)	9 (0.0)
21	3 (0.0)	7 (1.0)	9 (0.0)
24	7 (0.0)	8 (1.0)	9 (0.0)

These mixtures are linear combinations of 3 aerosol models in terms of fractional AOD.

This procedure is repeated using the TOA radiances of all spectral bands. It is important to note that in theory the retrieved $\beta_{e,in}$ (550 nm) does not depend on the choice of the spectral band because the radiance simulated over the full wavelength range is parameterized by β_e (550 nm).

3.2.2. Retrieval of surface and aerosol optical properties using MISR radiance measurements under real atmospheric conditions

In reality, the aerosol composition and size distribution, the vertical aerosol profile, clouds, and the bidirectionality of the surface reflectance are not exactly the same as pre-defined in the

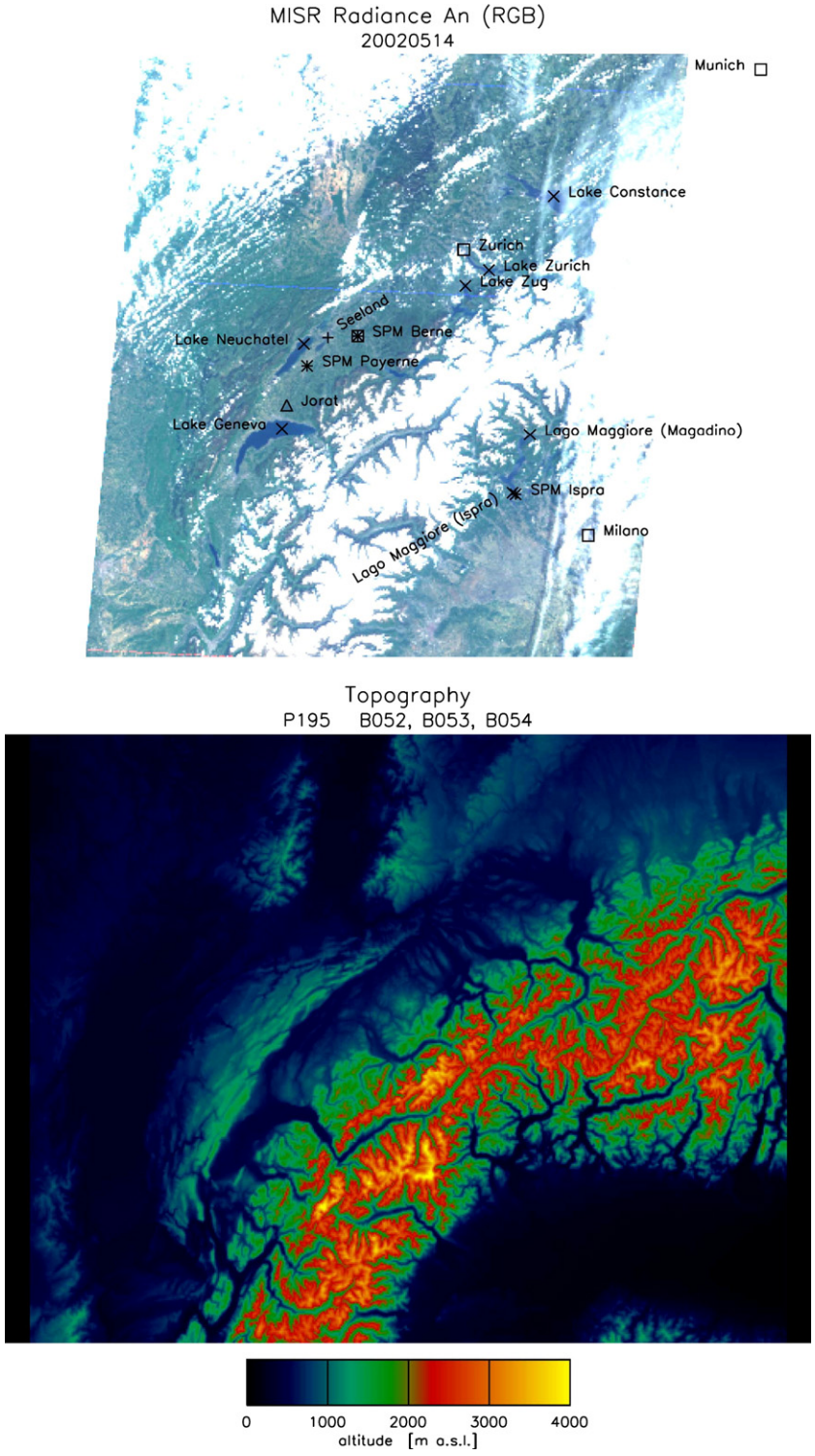

Fig. 4. Top: RGB MISR radiance image of the nadir looking camera An for blocks 52–54. May 14, 2002, path 195. Locations of the targets mentioned in the text: water (x), agriculture (+), forest (Δ), city (❑), sun photometers (*). Bottom: topography.

RTM. Due to this mismatch, the characteristic functions are expected not to intersect at one single point. However, for a clear sky and atmospheric conditions close to those of the RTM the intersections usually cluster in a common area.

The first objective is to calculate a representative data pair [$\beta_{e,in}$ (550 nm), $\rho_{surf,in}$] using the radiances of each of the 4 spectral bands separately. For each band, $n=(9\times8)/2=36$ intersections are possible. Representative values of $\beta_{e,in}$ (550 nm) and $\rho_{surf,in}$ are computed as weighted averages of the individual intersections, the weights being the inverse square of their uncertainties. Only those intersections are considered for which $\beta_{e,in}$ (550 nm)>0 and $\rho_{surf,in}>0$ holds.

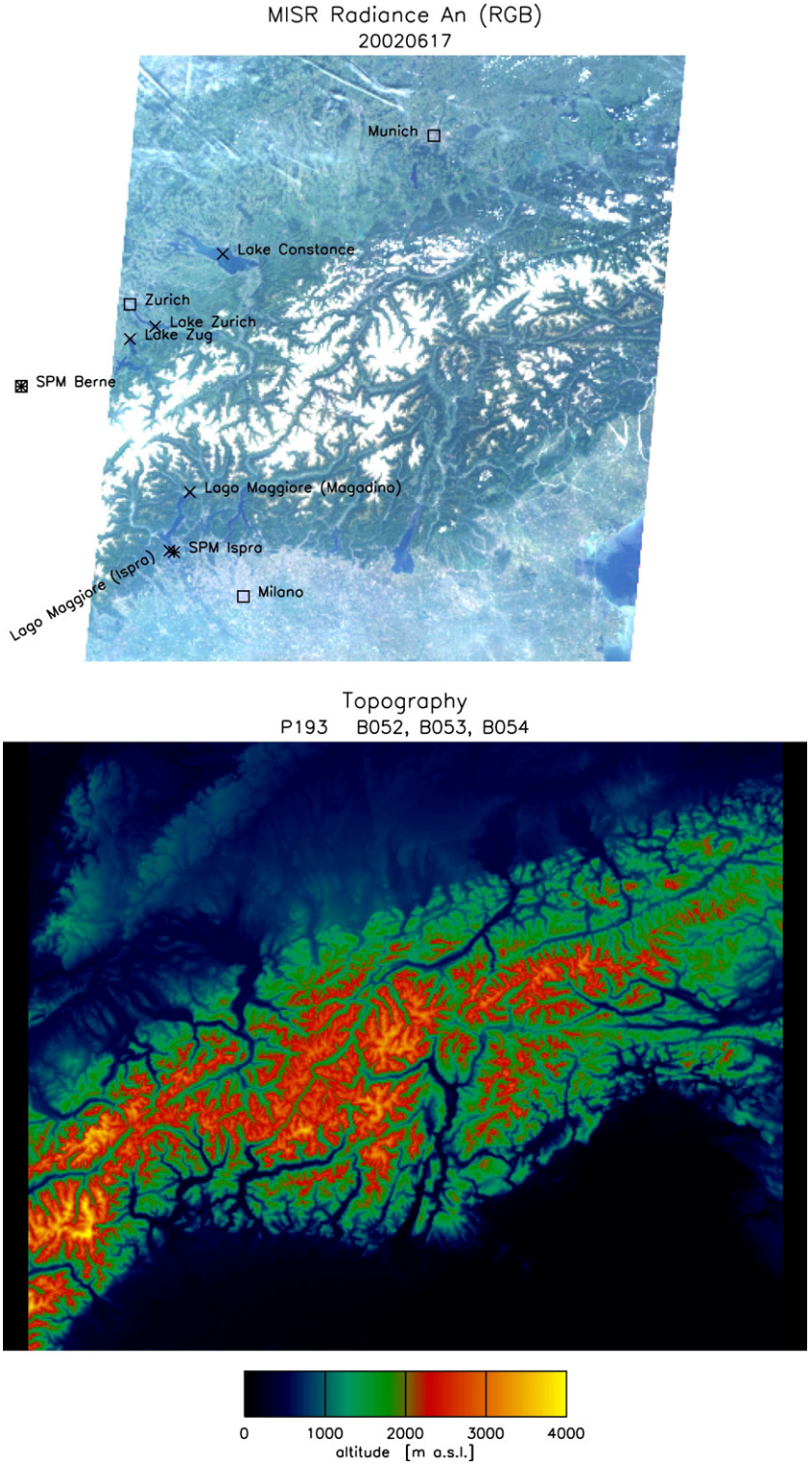

Fig. 5. Top: RGB MISR radiance image of the nadir looking camera An for blocks 52–54. June 17, 2002, path 193. Locations of the targets mentioned in the text: water (x), agriculture (+), forest (Δ), city (❑), sun photometers (*). Bottom: topography.

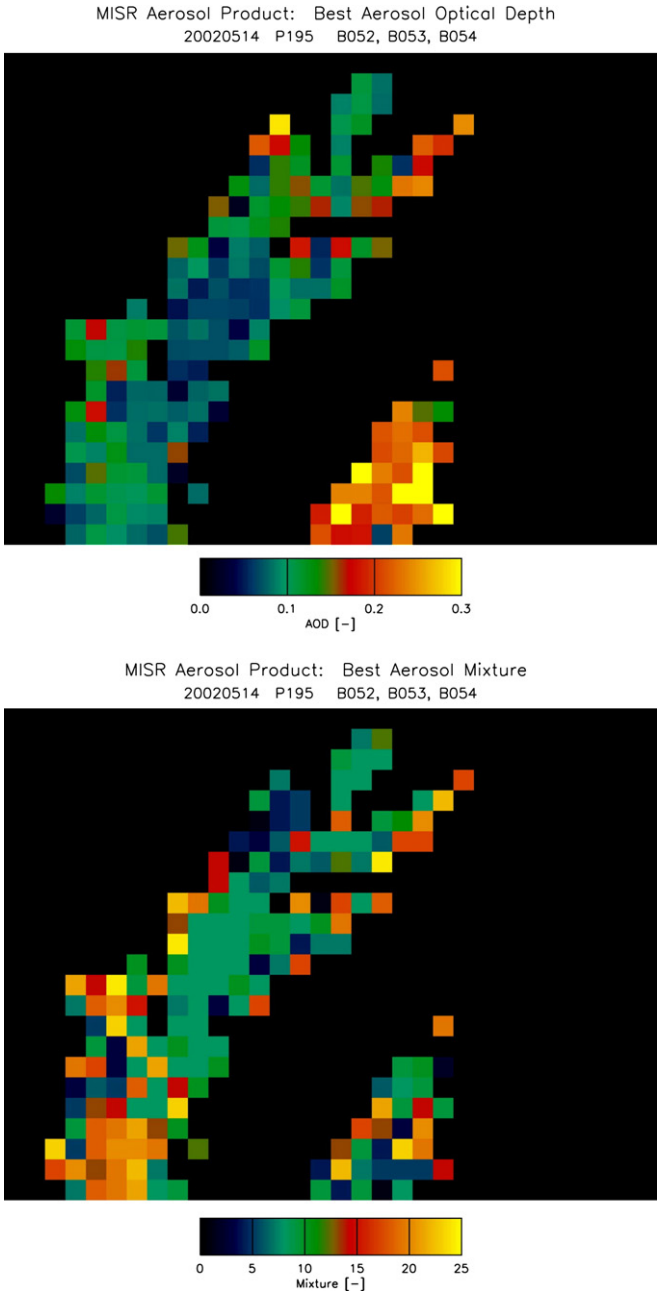

Fig. 6. Top: regional mean AOD (557 nm) of the MISR Aerosol Product. Bottom: aerosol mixture. May 14, 2002 (low aerosol load), blocks 52–54, path 195.

Perturbed conditions, e.g. due to clouds, are disregarded by this pre-selection.

The in-flight calibration file INFLTCAL of the MISR Ancillary Radiometric Product (ARP) provides percentage calibration uncertainties of each camera and band. As an example, the relative radiance uncertainty of each camera at the equivalent reflectance $\rho_{eq}=L_{MISR}(\lambda,\text{cam})/E_0=0.1$ is 3.4%. The camera-to-camera uncertainty given for $\rho_{eq}=0.1$ is 3.2%. These percentages are used to derive the uncertainty of $L_{MISR}(\lambda,\text{cam})$. As an example, Fig. 3 shows the characteristic functions of the cameras Df and Bf (solid lines). The increase or decrease of the respective radiances by their uncertainties results in a shift of the respective functions (dashed lines). There is a common area subtended by the uncertainty lines $\rho_{surf}\pm\Delta\rho_{surf}$ of each camera (hatched area). The maximum extensions of this area projected on the β_e (550 nm) and ρ_{surf} axes were taken as a measure for the uncertainties of $\beta_{e,in}$ (550 nm) and $\rho_{surf,in}$, respectively.

The most likely values for $\beta_{e,in}$ (550 nm)>0 and $\rho_{surf,in}>0$ are computed as the weighted average of a subset of these positive intersections, their weights being $(\Delta\beta_{e,in}\ (550\ \text{nm}))^{-2}$ and $(\Delta\rho_{surf,in})^{-2}$, respectively. This subset is selected by the following procedure. First, the most likely β_e (550 nm) is determined by a histogram analysis using a bin size of

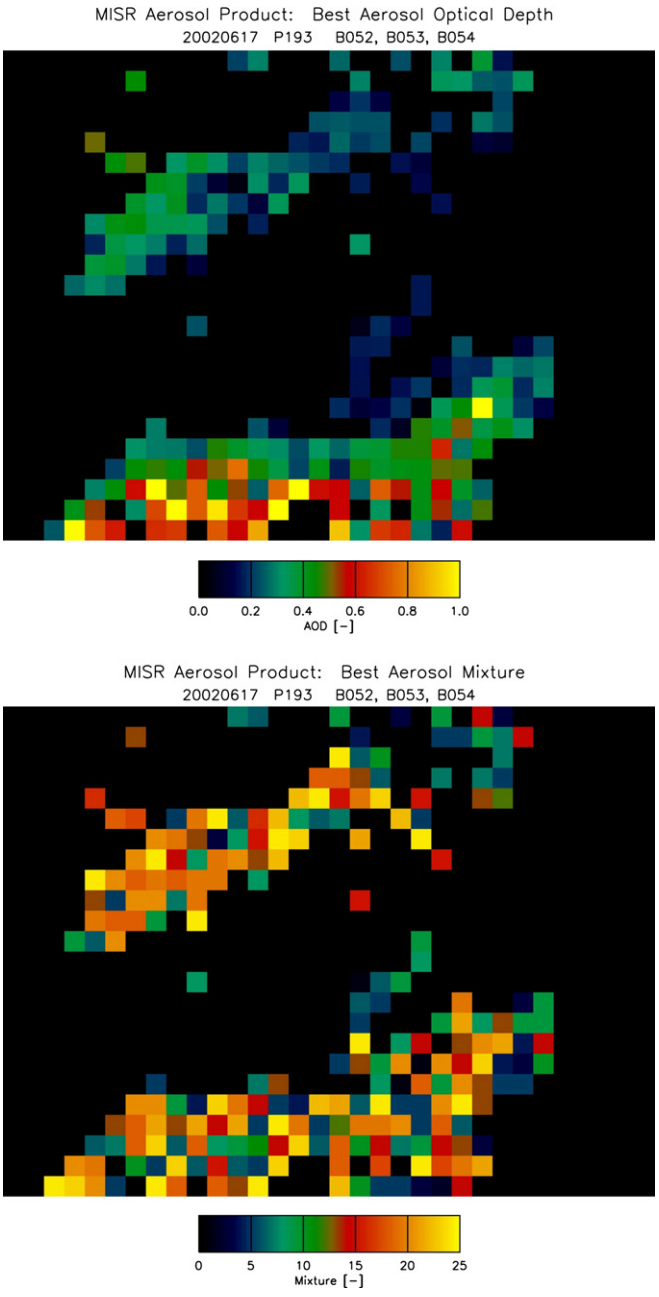

Fig. 7. Top: regional mean AOD (557 nm) of the MISR Aerosol Product. Bottom: aerosol mixture. June 17, 2002 (high aerosol load), blocks 52–54, path 193.

0.02 km^{-1} (see Fig. 11). All intersections within the interval $\beta_{e,bin}$ (550 nm)±0.02 km^{-1} are considered, where $\beta_{e,bin}$ (550 nm) is the center value of the most probable bin. Cameras with outlier intersections are disregarded by this procedure. We require that for a successful retrieval at least $n=4$ intersections must be located within this interval. The retrieved values $\overline{\beta_{e,\lambda}}$ (550 nm) and $\overline{\rho_{surf,\lambda}}$ for each MISR spectral band λ are calculated as weighted averages of the selected $\beta_{e,in}$ (550 nm) and $\rho_{surf,in}$. $\overline{\beta_{e,\lambda}}$ (550 nm) is subsequently used to interpolate the vertical transmittance LUT to get the vertical AOD.

Disturbed conditions, for instance in cloudy areas, are characterized by functions without any significant intersection cluster. Hence, this selection procedure is capable of masking out cloudy subregions.

We already mentioned that the retrieval algorithm should yield the same $\overline{\beta_{e,\lambda}}$ (550 nm) for each MISR spectral band λ if the parameters of aerosol mixture used as input data for MODTRAN 4 were identical to those of the real atmosphere. In practice, $\overline{\beta_{e,\lambda}}$ (550 nm) varies with wavelength due to the mismatch of the real aerosol properties and those used in the radiative transfer simulations. However, an optimum mixture can be derived. For this mixture the scatter of the intersections $\overline{\beta_{e,\lambda}}$ (550 nm) computed for the four spectral bands is minimal. The average extinction coefficient $\overline{\beta_e}$ (550 nm) is calculated as the weighted average of the coefficients $\overline{\beta_{e,\lambda}}$ (550 nm), the weights being the inverse squares of the uncertainties of $\overline{\beta_{e,\lambda}}$ (550 nm). The optimum AOD (550 nm) is calculated by a similar averaging procedure.

3.2.3. Aerosol composition and profile

The MISR Aerosol Climatology Product (ACP) was used to specify the physical properties of aerosols (Lewicki et al., 2003; NASA/ASDC, 2002). Version 2.2 data of the Aerosol Physical and Optical Properties (APOP) and of the Aerosol Mixture (MIXTURE) were taken from the data files MISR_AM1_ACP_APOP_F03_0004.hdf and MISR_AM1_ACP_MIXTURE_F03_0006.hdf, respectively. The most important parameters of the 11 aerosol models are listed in Table 1. The proportions of the 3 models contributing to those

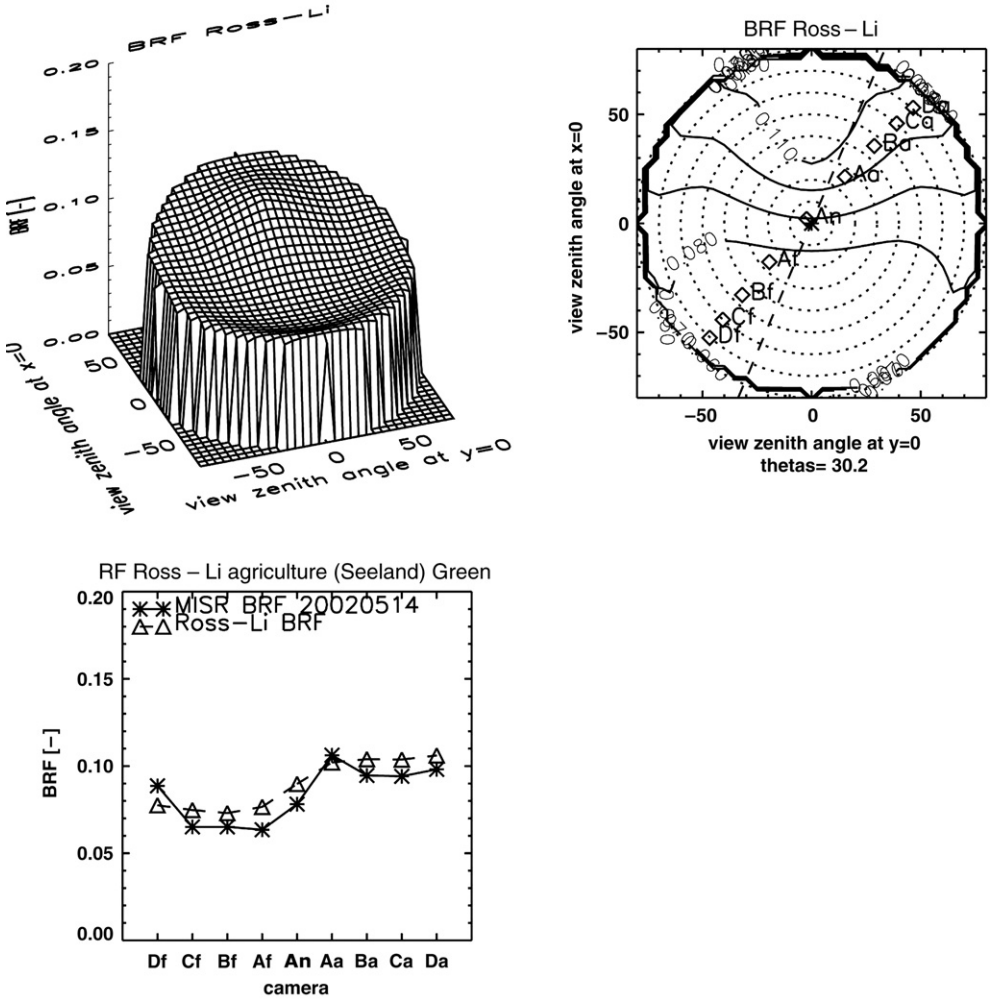

Fig. 8. Bidirectional Reflectance BRF for the agriculture site "Seeland" on May 14. Top left panel: Ross–Li surface plot for $P_1=0.10$, $P_2=0.01$ and $P_3=0.10$. Top right panel: contour plot: BRF contour lines (—); contour lines of equal view zenith angles (‴); north–south direction (- - -); view geometry of the MISR cameras Df to Da (◇). Bottom left panel: BRF of the MISR surface product (*); Ross–Li BRF (Δ).

mixtures used in this study are given in Table 2. Note that the proportions are defined as fractional optical depths and not as fractional particle masses or numbers.

The vertical aerosol profile was divided in a tropospheric and a stratospheric (background) section. In the troposphere a constant extinction coefficient up to the top z_{top} of the mixing layer was assumed. For subregions at higher altitudes h, z_{top} is scaled according to

$$z_{top}(h) = z_{top}(h=0)(h_{max}-h)/h_{max},$$

where h_{max}=6 km a.s.l. At sea level z_{top} (h=0)=1500 m a.g.l. was chosen as first guess. This value is supported by airborne lidar observations over the eastern Po Basin (Nyeki et al., 2002). Radiosonde soundings at Payerne (490 m a.s.l.) suggest mixing layer heights of about 2600 and 980 m a.s.l. on May 15 and June 17, 2002, respectively. Over large lakes this height is usually less. Values of about 1000 m a.s.l. were derived from Udine (114 m a.s.l.) soundings on both days. Measurements at Milano–Linate (98 m a.s.l.) yield about 400 and 750 m a.s.l. on May 15 and June 17, 2002, respectively. We show in Section 4.2. that a decrease of the assumed sea level z_{top} increases the retrieved extinction coefficient. The AOD, however, does not change substantially. z_{top} has to be adapted to real atmospheric profiles later.

The stratospheric extinction coefficient was taken from the MODTRAN 4 built-in profiles and the optical properties from mixture 24. From Tables 1 and 2 it is evident that this mixture contains only aerosol model 8, which is supposed to be representative for heights up to 10 km. We compared sun photometry data taken on a day with low aerosol concentrations (May 14) at the high-alpine site Jungfraujoch (3580 m a.s.l.) in Switzerland with the built-in background AOD (550 nm). AOD (550 nm)=0.03 was measured by the sun photometer, whereas AOD (550 nm)=0.09 was found for the built-in profile. Hence, we scaled the background profile by 0.3 to get a better agreement with the measurements.

3.2.4. Bidirectional Reflectance Factor (BRF)

The BRF characterizes the reflectance of a surface as a function of the sun's and the viewer's position angles. It is defined

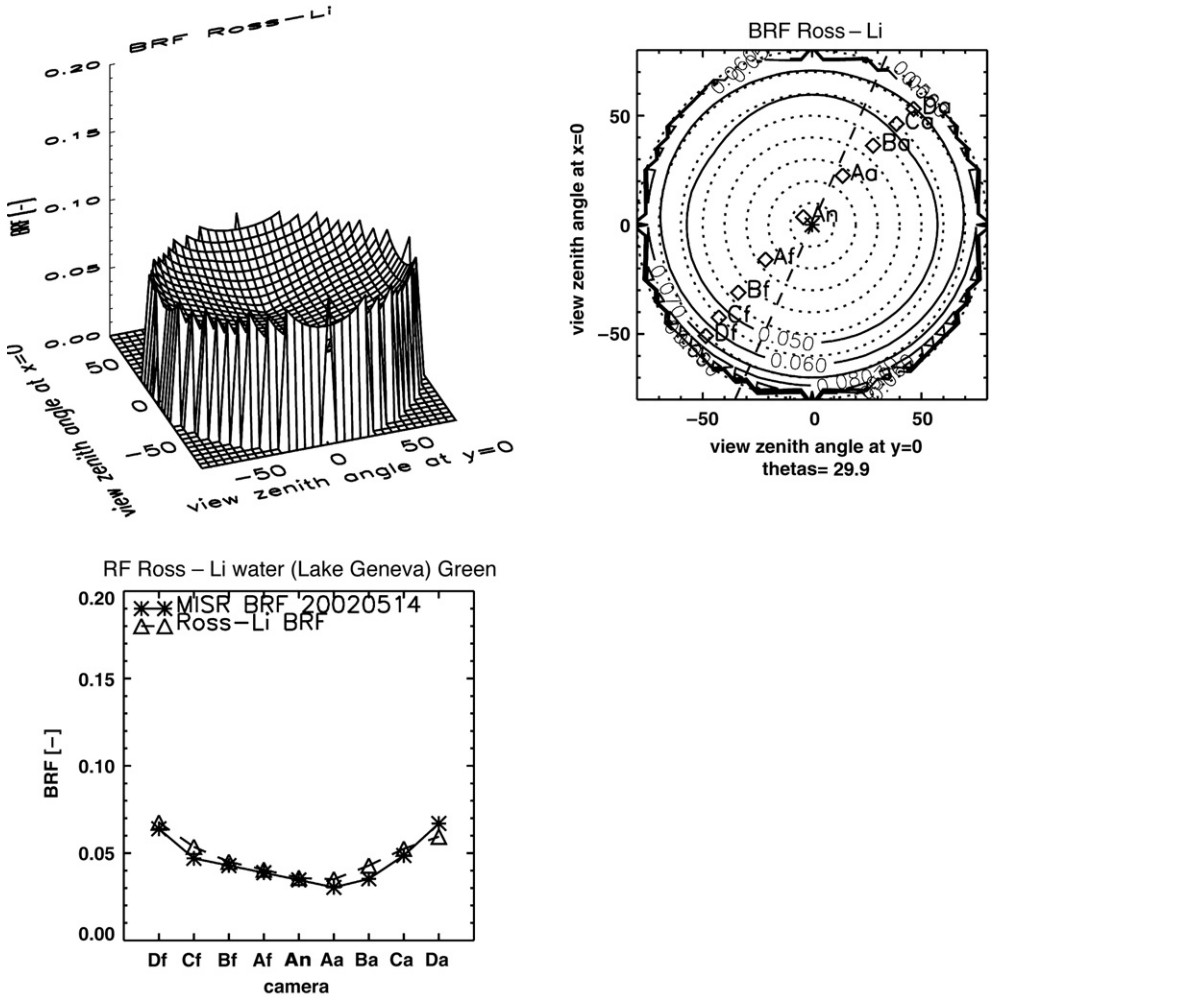

Fig. 9. Bidirectional Reflectance BRF for the water site "Lake Geneva" on May 14. Top left panel: Ross–Li surface plot for P_1=0.025, P_2=−0.015 and P_3=0.040. Top right panel: contour plot: BRF contour lines (—); contour lines of equal view zenith angles (‴); north–south direction (- - -); view geometry of the MISR cameras Df to Da (◇). Bottom left panel: BRF of the MISR surface product (*); Ross–Li BRF (Δ).

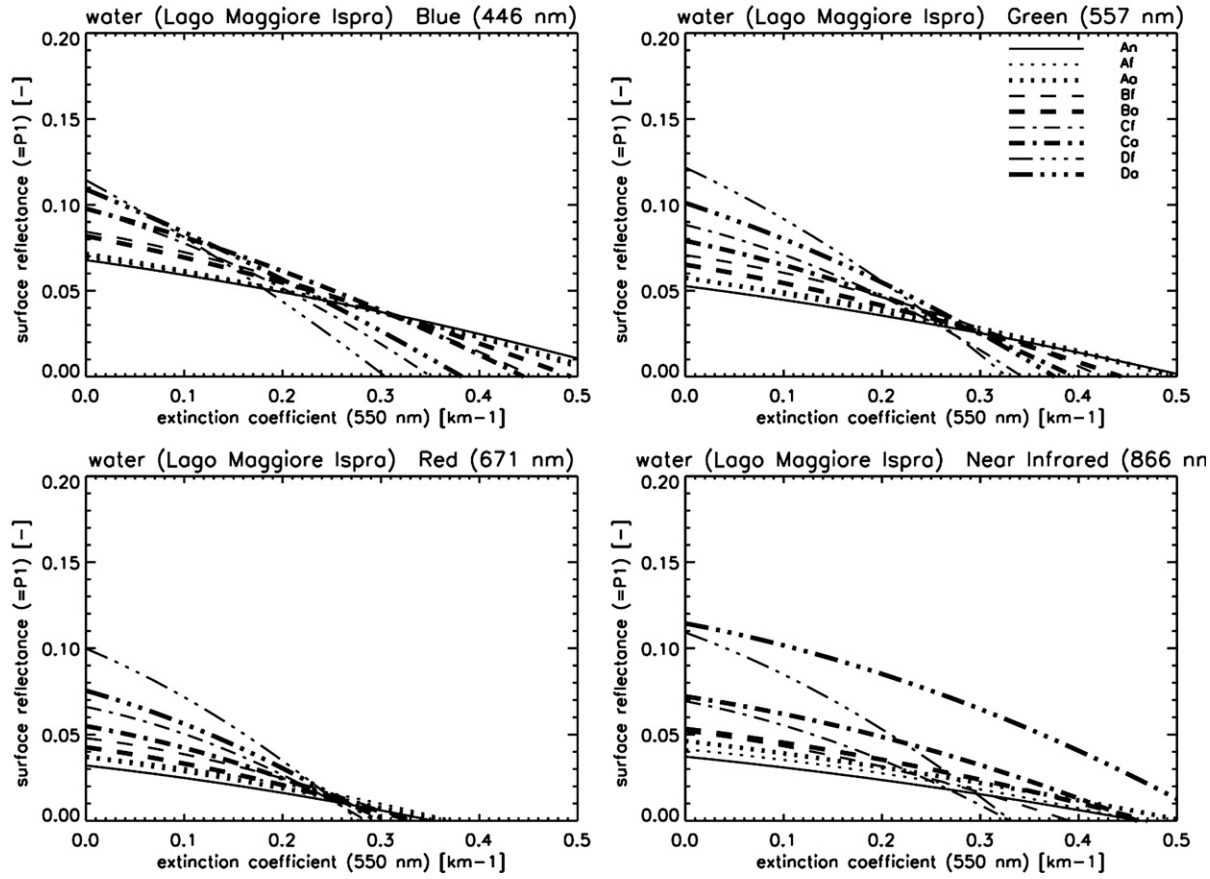

Fig. 10. Surface reflectance ρ_{surf} vs. ground level aerosol extinction coefficient β_e (550 nm) for the water target Lago Maggiore close to Ispra. The MISR radiances of the 4 MISR bands for June 17, 2002 and the look-up tables for the optimum mixture 18 were used to derive these functions. A Lambertian surface reflectance was assumed.

as "surface-leaving radiance divided by incident radiance from a Lambert reflector illuminated from a single direction". Hence, the BRF of a Lambertian surface is equal to its reflectance. Comprehensive compilations of the most important angular functions are given in Nicodemus et al. (1977) and Martonchik and Bruegge (2000).

There are numerous semi-empirical and physical BRF models with different parameterization available. The operational MISR

Table 3
Sensitivity of the extinction coefficient and the AOD at 550 nm to the choice of the aerosol mixture

Mixture	$\overline{\beta_{e,\lambda}}$ (550 nm) (km^{-1})				$\overline{\beta_e}$ (550 nm) (km^{-1})	$\Delta\overline{\beta_e}$ (550 nm) (%)	$\overline{AOD}$ (550 nm) (−)	$\Delta\overline{AOD}$ (550 nm) (%)
	Band 1	Band 2	Band 3	Band 4				
1	0.045±0.004	0.093±0.006	0.114±0.008	–[1]–	0.072±0.016	23.0	0.141±0.015	10.4
3	0.066±0.009	0.167±0.008	0.206±0.005	0.353±0.005	0.186±0.026	14.1	0.234±0.007	2.9
5	0.246±0.037	0.230±0.011	0.249±0.007	0.333±0.012	0.260±0.016	6.2	0.341±0.007	2.2
7	0.213±0.033	0.236±0.018	0.228±0.010	0.280±0.009	0.252±0.016	6.3	0.395±0.016	3.9
8	0.177±0.042	0.242±0.019	0.215±0.011	0.262±0.011	0.236±0.014	6.0	0.389±0.021	5.5
9	0.203±0.028	0.173±0.022	0.194±0.008	0.233±0.009	0.209±0.012	6.0	0.284±0.004	1.4
10	0.071±0.011	0.148±0.016	0.161±0.015	0.212±0.010	0.149±0.034	22.6	0.232±0.009	4.0
11	0.053±0.006	0.110±0.010	0.162±0.013	–[1]–	0.080±0.022	26.8	0.177±0.006	3.6
12	0.052±0.009	0.173±0.008	0.204±0.010	0.493±0.062	0.141±0.037	26.1	0.241±0.022	9.2
13	0.114±0.021	0.214±0.011	0.270±0.008	0.493±0.030	0.249±0.022	8.9	0.317±0.009	3.0
15	0.233±0.046	0.364±0.030	0.311±0.022	0.372±0.037	0.327±0.017	5.3	0.427±0.036	8.4
17	–[1]–	0.450±0.037	0.291±0.024	0.371±0.015	0.359±0.021	5.9	0.521±0.024	4.5
18	**0.308±0.054**	**0.291±0.022**	**0.250±0.007**	**0.275±0.012**	**0.259±0.008**	**3.0**	**0.355±0.011**	**3.2**
21	–[1]–	0.396±0.032	0.245±0.008	0.192±0.007	0.221±0.019	8.8	0.383±0.026	6.9

Data were simulated for June 17, 2002 at the Lago Maggiore site close to Ispra. $\overline{\beta_{e,\lambda}}$ (550 nm): extinction coefficient at 550 nm averaged over the intersections calculated for the MISR radiances of band 1,2, 3 and 4 (see text for details). $\overline{\beta_e}$ (550 nm) weighted average of $\overline{\beta_{e,\lambda}}$ (550 nm), $\overline{AOD}$ (550 nm): weighted average of AOD. Mixture 18 yields extinction coefficients that scatter least (bold). [1] Insufficient number of valid data points.

land surface product includes BRF data for each subregion (1.1 km) supplemented by the 3 best-fit parameters of a modified version of the Rahman–Pinty–Verstraete (RPV) model (Rahman et al., 1993).

MODTRAN 4 supports 9 different BRF models, including the RPV approach. The RPV model is appropriate for vegetation, but it is not possible to describe a Lambertian reflector correctly for any geometric configuration. Zenith angles must be set to 0 to obtain Lambertian reflectance. This drawback is overcome in the Ross–Li approach (Lucht et al., 2000; Wanner et al., 1995, 1997), where the angular dependence of the radiation in a canopy is described with 5 parameters P_1 to P_5. The equation for the BRF is composed of 3 terms:

$$\rho_{\mathrm{surf}}(\theta_v,\theta_s,\Delta\varphi) = P_1 + P_2\ K_{\mathrm{LSR}}(\theta_v,\theta_s,\Delta\varphi,P_4,P_5) + P_3\ K_{\mathrm{RT}}(\theta_v,\theta_s,\Delta\varphi),$$

where θ_v, and θ_s are the view and the solar zenith angle, respectively. $\Delta\varphi$ is the view azimuth angle relative to the sun's position. K_{LSR} and K_{RT}, which are parameterized by P_4 and P_5, are kernels for geometric scattering at sparse objects on Lambertian ground and for volume scattering in a dense leaf canopy, respectively. $P_2{=}P_3{=}0$ reduces the reflectance to the Lambertian case $\rho_{\mathrm{surf}}{=}P_1$.

As mentioned above, the surface reflectance is varied to generate the look-up tables. In the non-Lambertian case, P_1 is varied, and the ratios P_2/P_1 and P_3/P_1 are kept constant for a given surface type. More details of the choice of P_1, P_2 and P_3 are given in Section 4.2.

4. Results

We tested the simultaneous retrieval (SR) algorithm for Switzerland and northern Italy. Blocks 52 to 54 of the MISR overpass paths 192–198 partly include Switzerland. MISR follows one of these paths every 2nd to 5th day. From all possible paths in summer 2002 with clear sky conditions we selected 2 days according to their different aerosol concentrations: May 14 was a relatively clear day with low aerosol concentrations. On June 17 a substantial aerosol load was observed. These days have been selected on the basis of sun photometer records and ground level PM10 measurements.

The respective RGB radiance images and the topography for the 2 days are depicted in Figs. 4 and 5. Blocks 52 and 54 are horizontally shifted by 16 subregions (i.e. 1 region) to the right and to the left, respectively. The locations of the water, agriculture, forest and sun photometer (SPM) targets used in the analysis are indicated as well.

Figs. 6 and 7 shows the MISR regional mean AOD (top) and mixture (bottom) of the blocks 52 to 54 for May 14 (low aerosol load) and June 17 (high aerosol load), respectively. Differences in AODs north and south of the Alps are clearly evident. Note the different scales used for the 2 days.

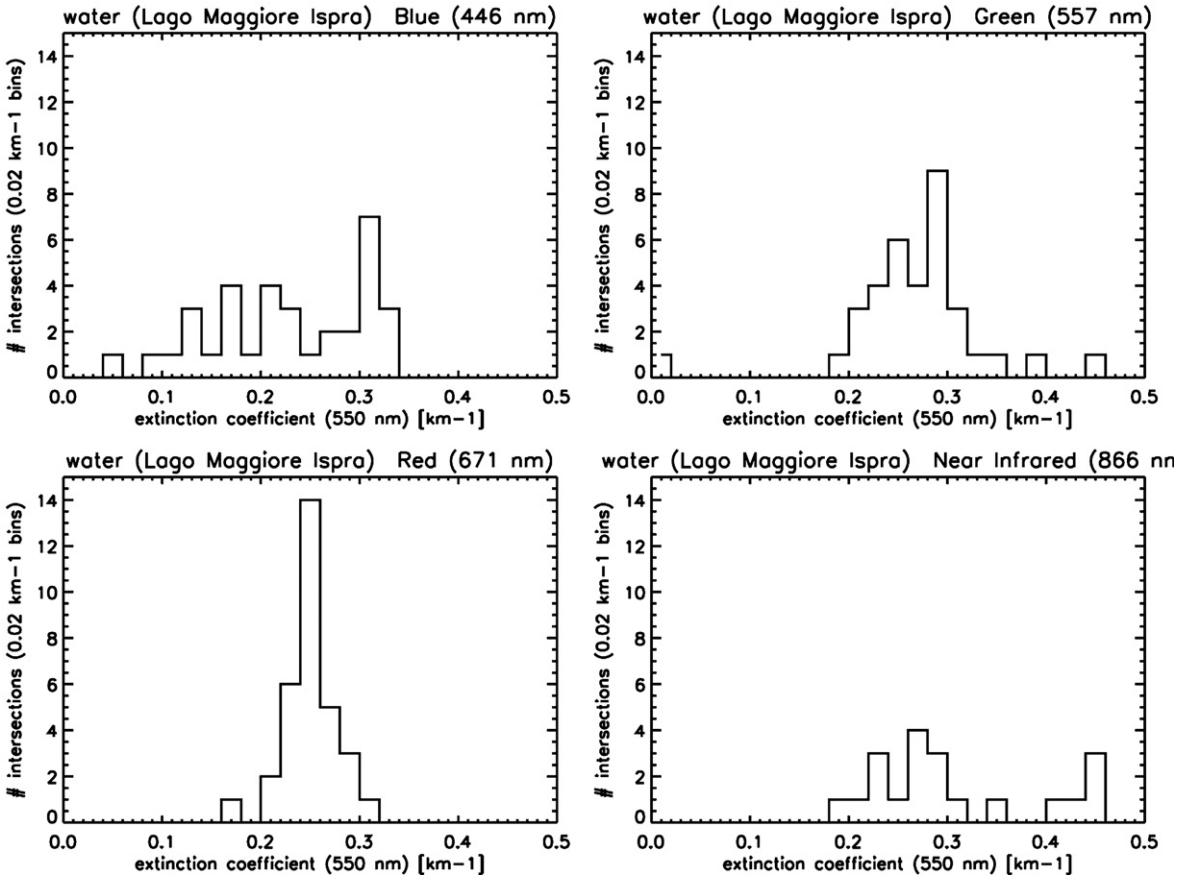

Fig. 11. Histograms of the intersection extinction coefficients $\beta_{e,in}$ (550 nm) of Fig. 10.

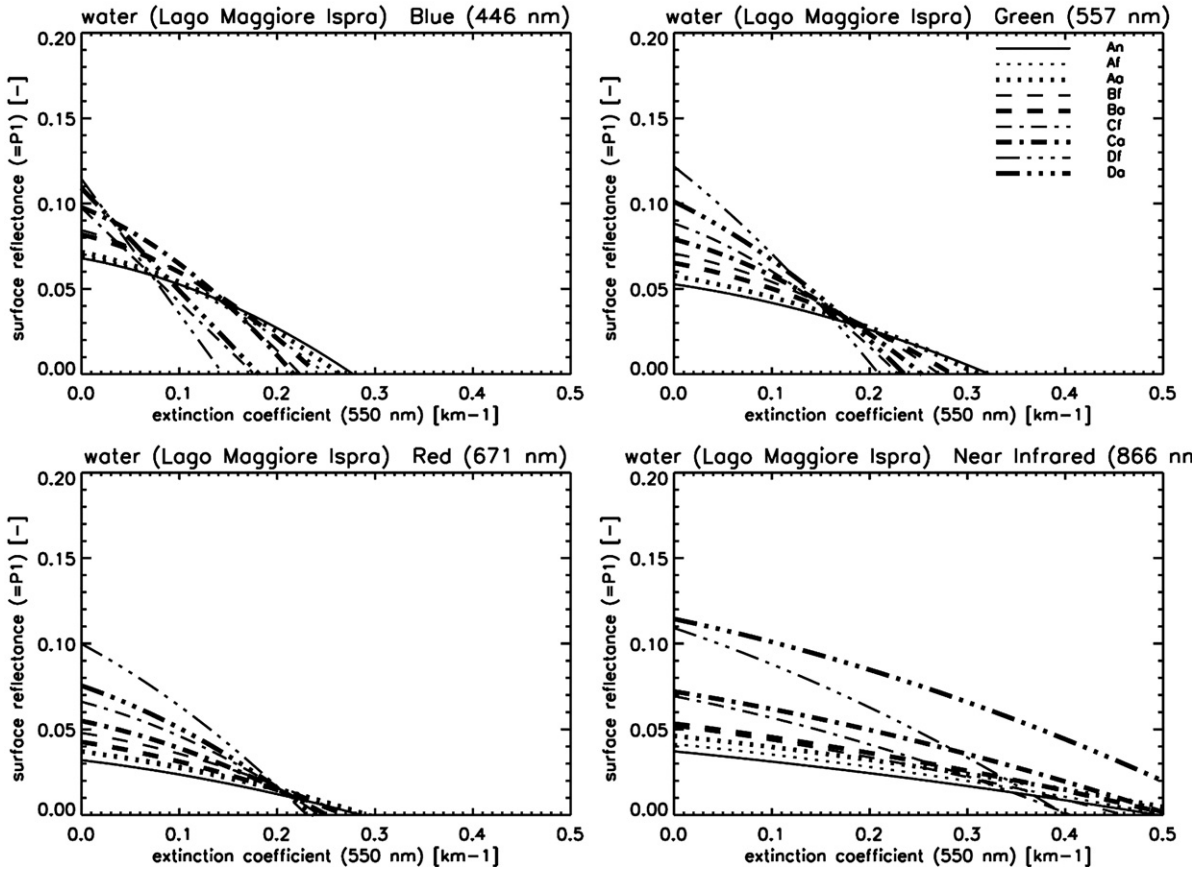

Fig. 12. Surface reflectance ρ_{surf} vs. ground level aerosol extinction coefficient β_e (550 nm) for the water target Lago Maggiore close to Ispra. The MISR radiances of the 4 MISR bands for June 17, 2002 and the look-up tables for mixture 3 were used to derive these functions. A Lambertian surface reflectance was assumed.

4.1. Sun photometry

In order to compare the AODs provided by the MISR standard aerosol product and by the SR algorithm with sun photometer (SPM) measurements, data from stations in Switzerland and in the Po Basin were taken.

For the Swiss area, data from the Institute for Applied Physics at University of Berne and the Swiss Atmospheric Radiation Measurement Network (IAP/CHARM) were used for the Berne and Payerne locations. The Berne aerosol optical depth is given in 10 channels ranging from 340 to 1024 nm, at 30 s sampling intervals during sunshine. Equally sampled, the Payerne data are defined in four channels between 368 and 862 nm. The AERONET station Ispra (Holben et al., 1998) represents the Po Basin. The sun photometer data are reported in six channels at 440, 500, 535, 670, 870, and 1020 nm, given in 10 min averages. Uncertainties range between 2–5% for the IAP/CHARM, and less than 1% for the AERONET. AOD values relevant for the comparison of satellite-based data are included in Table 4.

4.2. Simultaneous retrieval algorithm

4.2.1. Bidirectional reflectance factor

To test the applicability of the Ross–Li model to different land cover types, we selected the following prototype locations: agriculture (Seeland), water (Lake Geneva) and forest (Jorat). For these locations, we adjusted the Ross–Li parameters P_1, P_2 and P_3 to values for which the BRFs of the 9 MISR cameras agrees best with the respective values of the operational surface product. Fig. 8 shows the main features of the BRF for Seeland on May 14. Surface and contour plots for $P_1=0.10$, $P_2=0.01$ and $P_3=0.10$ ($P_2/P_1=0.1$, $P_3/P_1=1.0$) are depicted in the top left and top right panel, respectively. The “hot spot” and the symmetry relative to the principal plane, i.e. relative to the light source, are clearly visible. The contour plot includes the view angles of the cameras Df to Da as well as the south direction (dashed line). In the bottom panel the BRF values for the 9 cameras calculated with the Ross–Li model are compared with those of the operational surface product. For the sensor and target angles valid for the time and location of interest, camera Aa points closest to the hot spot. Note that it is impossible to obtain a perfect agreement for all cameras. For the forest site Jorat $P_1=0.055$ was found. It is important to note that the same ratios $P_2/P_1=0.1$ and $P_3/P_1=1.0$ as for agriculture were obtained.

Ocean water is not a Lambertian reflector because of the sun glint, the wind dependent shape of the waves and the formation of white caps (Cox & Munk, 1955). Wind speeds over inland water bodies in Switzerland, however, are usually much smaller that those over open oceans, leading to lower waves and less white caps. Hence, we assumed the lake water to be Lambertian.

Table 4
Comparison of the best-fit AOD (550 nm) and mixture derived by the simultaneous retrieval (SR) method with the regional mean AOD and mixture of the MISR aerosol product, and with sun photometer AOD

Date/site	$\overline{\text{AOD}}$ (550 nm) (SR method)	Mixture (SR method)	AOD (557 nm) (MISR)	Mixture (MISR)	AOD (550 nm) (SPM)
May 14, 2002					
Lake Geneva	0.086±0.002	8	0.067±0.023	8	
Lake Neuchatel	0.082±0.004	5	0.056±0.013	8	
Lake Zug	0.243±0.022	18	n.a.	n.a.	
Lake Zurich	0.260±0.024	9	n.a.	n.a.	
Lake Constance	0.375±0.008	8	n.a.	n.a.	
Lago Maggiore (Magadino)	0.188±0.010	9	n.a.	n.a.	
Lago Maggiore (Ispra)	0.203±0.019	5	0.228±0.044	5	
SPM Payerne	n.a.		0.076±0.024	10	0.02±0.001
SPM Bern	n.a.		0.083±0.029	17	0.06±0.003
SPM Ispra	0.127±0.002	5	0.228±0.044	5	0.20±0.002
June 17, 2002					
Lake Geneva	n.a.	n.a.	n.a.	n.a.	
Lake Neuchatel	n.a	n.a.	n.a.	n.a.	
Lake Zug	0.320±0.010	18	n.a.	n.a.	
Lake Zurich	0.319±0.005	8	n.a.	n.a.	
Lake Constance	0.339±0.007	8	n.a.	n.a.	
Lago Maggiore (Magadino)	0.371±0.006	15	0.747±0.206	5	
Lago Maggiore (Ispra)	0.355±0.011	18	0.386±0.102	18	
SPM Payerne	n.a	n.a.	n.a.	n.a.	0.33±0.020
SPM Bern	n.a.	n.a.	n.a.	n.a.	0.28±0.010
SPM Ispra	0.094±0.003	7	0.386±0.102	18	0.42±0.004

The simultaneous retrieval algorithm assumes the BRF for agriculture when applied to the sun photometer sites. On May 14, 2002, no SR AOD was calculated because of negative retrievals of the extinction coefficient. On June 17, 2002, the MISR swath did not cover Lake Geneva, Lake Neuchatel, Berne and Payerne.

Sun glint effects are minimized by omitting data of cameras close to the glitter angle. In the operational surface product the BRF has a bowl shape (see Fig. 9). A satisfactory agreement would be achieved if the Ross–Li parameters were set to $P_1=0.025$, $P_2=-0.015$ and $P_3=0.04$. Further investigations are needed to figure out if MODTRAN 4 handles negative parameters correctly.

4.2.2. Aerosol and surface reflectance retrieval over water

We applied the SR algorithm to the MISR radiances acquired at 7 subregions that coincide with lake water (see Figs. 4 and 5). Lake Geneva, Lake Neuchatel, Lake Zug, Lake Zurich and Lake Constance are large or medium size lakes in the Swiss Plateau. Lago Maggiore is located partly in southern Switzerland and in northern Italy and is heavily influenced by the polluted air of the Po Basin. The southern tip of Lago Maggiore is close to the sun photometer station at Ispra.

First, we focused on the Lago Maggiore site close to Ispra. This choice enables to study both high and low aerosol concentrations and to compare MISR based AOD with sun photometer measurements. In the first step we analyzed the data acquired on the day with high aerosol load, June 17. LUTs were calculated for selected aerosol mixtures listed in Table 2.

We explained in Section 3 that the retrieval algorithm should yield an optimum mixture and an extinction coefficient for which the scatter of the band related $\overline{\beta_{e,\lambda}}$ (550 nm) is expected to be minimal. As an example, Fig. 10 shows the characteristic functions $\rho_{\text{surf}}=f_{\lambda,\text{cam}}$ (β_e (550 nm)) for the 4 spectral bands calculated for MISR aerosol mixture 18. This mixture was found to be the optimum case (bold numbers in Table 3). In Fig. 11 the histogram of the number of intersections in 0.02 km^{-1} bins are depicted. The green and the red band show a pronounced peak, whereas the distribution for the blue and the NIR band is broader. Short wave radiation is scattered most in the blue band. Due to this fact the mismatch of the mixture and the horizontal inhomogeneities are best visible in this band. In the NIR band the larger spread may be partly attributed to larger errors due to lower signal to noise ratio.

If the mixture selected for the LUT simulations differ significantly from the actual mixture, the scatter of $\overline{\beta_{e,\lambda}}$ (550 nm) becomes larger. The retrieved $\overline{\beta_{e,\lambda}}$ (550 nm) for fine particles, for instance present in mixture 3, are smaller and increase with wavelength (note the characteristic functions in Fig. 12). The extinction coefficient $\overline{\beta_{e,\lambda}}$ (550 nm) for band 1 to 4, the weighted average $\overline{\beta_e}$ (550 nm) calculated over those 4 bands and the optical depth $\overline{\text{AOD}}$ (550 nm) are listed in Table 3. As already mentioned, the smallest scatter leading to the lowest relative error of $\overline{\beta_e}$ (550 nm) was found for mixture 18 (bold numbers). For that mixture $\overline{\beta_e}$ (550 nm) and $\overline{\text{AOD}}$ (550 nm) equal 0.259±0.008 km^{-1} (3.0%) and 0.355±0.011 (3.2%), respectively. Note

Table 5
Best-fit extinction coefficient $\overline{\beta_e}$ (550 nm) and aerosol optical depth $\overline{\text{AOD}}$ (550 nm) as a function of the mixing layer height z_{top}

z_{top} (m a.g.l.)	$\overline{\beta_e}$ (550 nm) (km^{-1})	$\overline{\text{AOD}}$ (550 nm) (−)
500	0.668±0.023	0.360±0.014
1000	0.385±0.018	0.366±0.008
1500	0.259±0.008	0.355±0.011
2000	0.202±0.007	0.357±0.017

Mixture 18, June 17, 2002.

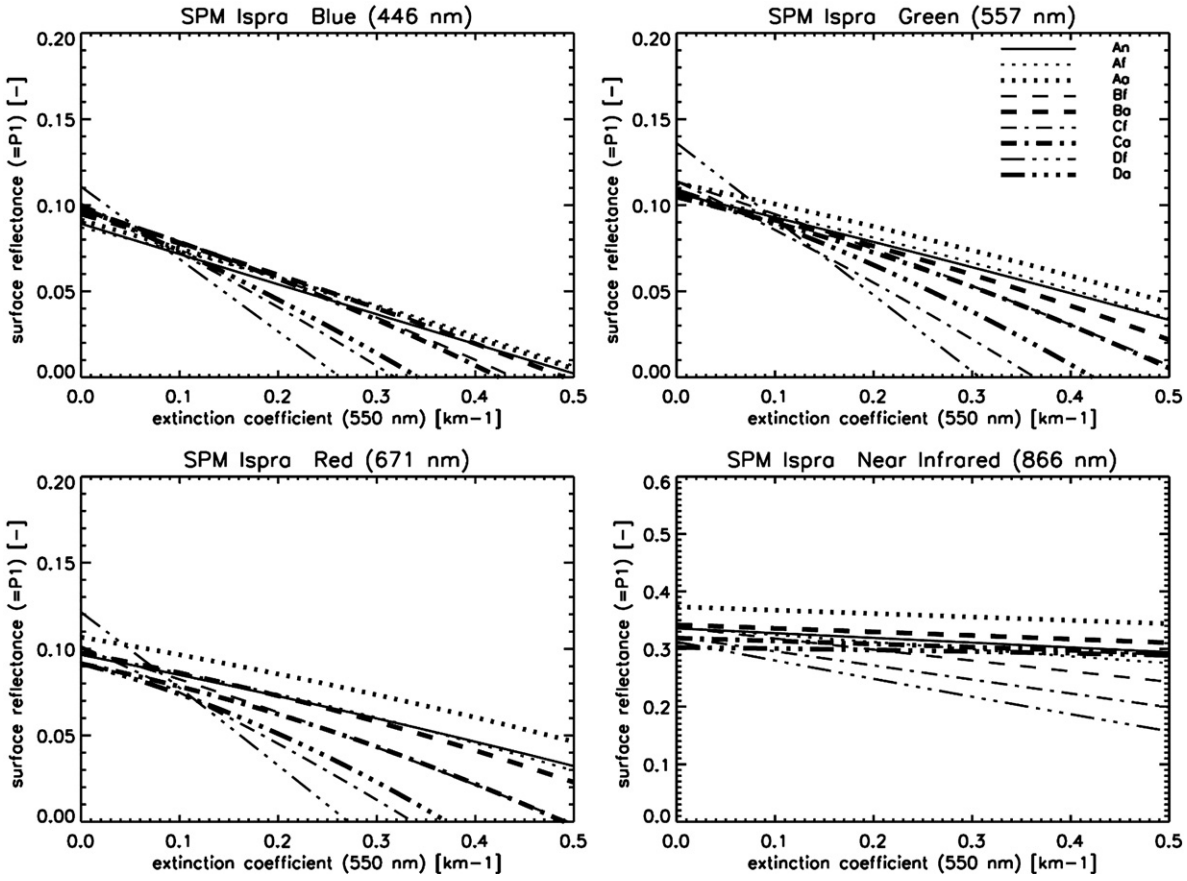

Fig. 13. Surface reflectance ρ_{surf} vs. ground level aerosol extinction coefficient β_e (550 nm) for the sun photometer target (vegetation) at Ispra. The MISR radiances of the 4 MISR bands for June 17, 2002 and the look-up tables for mixture 18 were used to derive these functions. A BRF for agriculture was assumed.

that $\overline{\beta_e}$ (550 nm) of mixture 18 is located within the intervals $\overline{\beta_e}$ (550 nm)$\pm\Delta\overline{\beta_e}$ (550 nm) of mixtures 5 and 7. We conclude that these 3 mixtures, which both contain substantial amounts of medium size particles, are not distinguishable. On the contrary, mixtures 1, 10, 11 and 12 are far from being optimal. They contain substantial amounts of ultrafine particles, which are not present in the optimum mixture 18.

At the beginning, we explained that all characteristic curves should intersect in one single point. We expected that the scatter of the intersections calculated for all cameras of one band and for the most realistic aerosol mixture should be minimal. However, the analysis of Table 3 shows that there are unrealistic mixtures that produce smaller deviations than mixture 18 (see e.g. band 2 of mixture 12). Hence, a small scatter of intersections is not an indicator for an optimum mixture.

The best-fit AOD retrieved over the 7 lake water targets are listed in Table 4 together with the MISR aerosol product, if applicable. Sun photometer measurements of Payerne, Bern and Ispra are included as well. On June 17, AOD at Lago Maggiore close to Ispra is about 8% less than the regional mean provided by the operational algorithm of MISR (0.386±0.102) and 15% less than the sun photometer measurements taken at Ispra (0.42±0.01). Note that the MISR operational algorithm retrieves mixture 18 as well.

As already mentioned, the mixing layer height z_{top} at sea level was specified as 1500 m a.g.l. To check the sensitivity of $\overline{\beta_e}$ (550 nm) and $\overline{AOD}$ (550 nm) with respect to z_{top}, the mixing layer height was changed to 500, 1000 and 2000 m a.g.l.. From Table 5 it is evident that $\overline{\beta_e}$ (550 nm) decreases with increasing z_{top}. $\overline{AOD}$ (550 nm), however, is nearly constant. This result is due to the fact that the vertical column densities of the aerosols confined to different volumes do not change. They backscatter more or less the same radiation to space regardless of their vertical distribution in the troposphere.

The surface reflectance values ρ_{surf} for the optimum mixture 18 calculated for the spectral bands 1 to 4 amount to 0.036± 0.009, 0.028±0.004, 0.013±0.001 and 0.022±0.002, respectively. This spectral dependence shows the well-known decrease of water reflectance with wavelength.

A second option to describe water reflectance is the use of the Ross–Li BRF as shown in Fig. 9. Remember that ρ_{surf} is no longer the Lambertian albedo but the Ross–Li parameter P_1. For mixture 7, for instance, the average values $\overline{\beta_e}$ (550 nm) and $\overline{AOD}$ (550 nm) amount to 0.207±0.012 km^{-1} and 0.334± 0.017, respectively. These numbers are 20% and 6% lower than those of the Lambertian assumption.

In the next step, we used MISR radiance data acquired on May 14 to test the capability of the algorithm for lower aerosol loads. At the Lago Maggiore site close to Ispra, the procedure yields mixture 5 as the optimum solution with $\overline{\beta_e}$ (550 nm)=0.165± 0.004 km^{-1} (2.7%) and $\overline{AOD}$ (550 nm)=0.203±0.019 (9.3%). The latter is again in good agreement with the corresponding

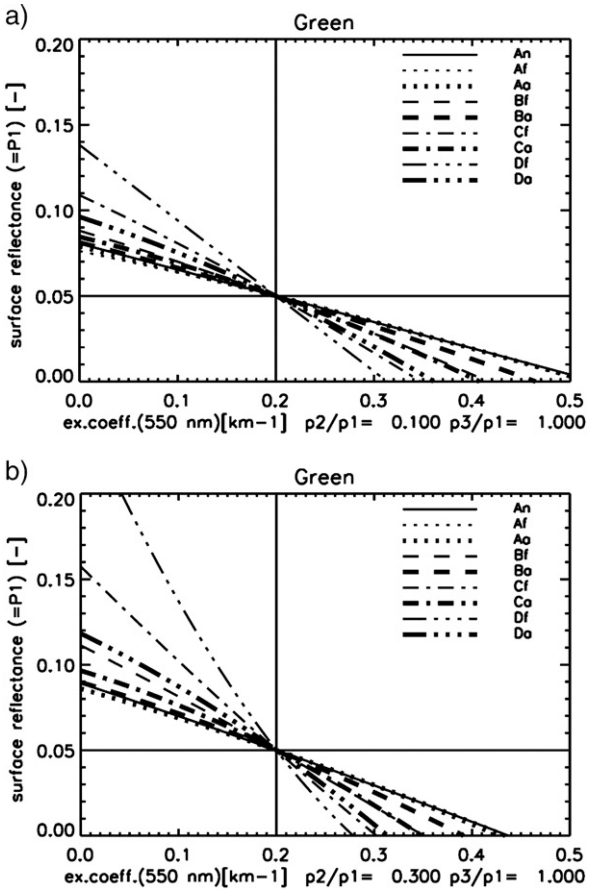

Fig. 14. Simulated surface reflectance ρ_{surf} vs. ground level aerosol extinction coefficient β_e (550 nm) for the MISR cameras Df to Da. The TOA radiance of each camera is kept constant for the full range of β_e (550 nm) and corresponds to the radiance of the green band at the reference values $\beta_{e,ref}$ (550 nm)=0.2 km^{-1} and P_1=0.05. a): BRF with P_2/P_1=0.1, P_3/P_1=1.0. b): BRF with P_2/P_1=0.3, P_3/P_1=1.0. See Fig. 2 for comparison with the Lambertian case and text for details.

AODs of the MISR aerosol product (0.228±0.044) and the Ispra sun photometer (0.20±0.002).

On May 14, the MISR path covered also Lake Geneva and Lake Neuchatel (Fig. 4). At the Lake Geneva test site, mixture 8 was found as the optimum ($\overline{\beta_e}$ (550 nm)=0.043±0.001 km^{-1} (3.2%) and $\overline{AOD}$ (550 nm)=0.086±0.002) (2.2%)). The MISR aerosol product reports a regional mean AOD of 0.067±0.023 for that site. The closest sun photometers are located at Payerne (for Lake Geneva and Lake Neuchatel) and Berne (for Lake Neuchatel). The AOD taken at Payerne is very low (0.02±0.001) compared to our data, whereas the measurement of Berne is in good agreement (Table 4).

From Figs. 4 and 5 it is evident that disturbances, e.g. due to clouds or contrails, are present. Due to the different scattering properties of these disturbances, the characteristic functions $\rho_{surf}=f_{\lambda,cam}$ (β_e (550 nm)) and their intersections become meaningless. Although this effect makes the retrieval of aerosol properties impossible, it might be used, at least partly, to mask out clouds.

4.2.3. Aerosol retrieval over vegetation

BRF parameters for agriculture were taken as typical for vegetation at the SPM station at Ispra. Fig. 13 shows the characteristic functions for mixture 18 on June 17. It is evident that the intersections are significantly shifted to smaller extinction coefficients compared with the data of the corresponding water target. This effect is even more pronounced for low aerosol loads (May 14), where $\beta_{e,in}$ (550 nm) of several intersections become negative. Although the intersections might be shifted to larger values by selecting larger particles, a change of the mixture over a distance of only a few kilometers seems unrealistic. Another possible way to fix this problem is to modify the contribution of the stratospheric aerosol. This would likely change the characteristic functions for low tropospheric aerosols. However, neither a decrease of the total stratospheric aerosol column nor a change of its composition leads to a sufficient shift of the intersections. Moreover, this modification affected the aerosol optical properties retrieved over water and over land by roughly the same amount.

It is obvious that the radiance LUTs and the characteristic functions depend on the selection of the BRF parameters. Similar to Fig. 2a ("reference" case, $\beta_{e,ref}$ (550 nm)=0.2 km^{-1}, $P_{1,ref}$=0.05) Fig. 14 depicts the characteristic functions for the agriculture target used in the analysis (P_2/P_1=0.1, P_3/P_1=1.0) and for a more pronounced hot spot (P_2/P_1=0.3, P_3/P_1=1.0). The respective functions tend to become steeper with increasing ratio P_2/P_1. We selected these 2 cases to retrieve $\overline{\beta_e}$ (550 nm) and $\overline{AOD}$ (550 nm) for the SPM Ispra site. For the extinction coefficient, $\overline{\beta_e}$ (550 nm)=0.048±0.002 and 0.134±0.004 km^{-1} were found. The respective $\overline{AOD}$ (550 nm) amount to 0.094±0.005 and 0.226±0.007. It is evident that the more pronounced hot spot results in larger values. However, this increase is not sufficient to reproduce the sun photometer measurements.

After numerous parameter variations without obtaining any reasonable best-fit extinction coefficients and AODs, we came to the conclusion that the radiative transfer model itself is likely the source for the incapability of the algorithm to retrieve aerosol optical properties over non-Lambertian targets. Recalling that the model is expected to describe the scattering processes in the atmosphere correctly, we suppose that the BRF formalism is not yet fully implemented in MODTRAN 4 v3r1. In Berk et al., 1999 the developers of MODTRAN 4 mention that in version v1r1 the BRF is only partly coupled with the DISORT N-stream model. The full coupling is not yet implemented in the current release v3r1 (Berk, 2005). We strongly recommend including this improved feature in the next update of MODTRAN 4. It is left to further investigations to retrieve improved aerosol optical properties using a modified MODTRAN 4 version.

Despite of these unsolved problems, we determined preliminary best-fit values $\overline{\beta_e}$ (550 nm) and $\overline{AOD}$ (550 nm) over vegetation at Ispra for June 17 in analogy to the retrieval procedure over water. Best-fit values were found for mixture 7 ($\overline{\beta_e}$ (550 nm)=0.048±0.002 km^{-1} (4.6%) and $\overline{AOD}$ (550 nm)=0.094±0.003 (3.6%)). The extinction coefficient, however, is about 0.2 km^{-1} less than $\overline{\beta_e}$ (550 nm) for the same mixture over water (0.252 km^{-1}). On May 14, mixture 5 (i.e. the same mixture as found over water) fits best at Ispra with $\overline{\beta_e}$ (550 nm)=0.069±0.001 km^{-1} (2.1%) and $\overline{AOD}$ (550 nm)=0.127±0.002 (1.7%).

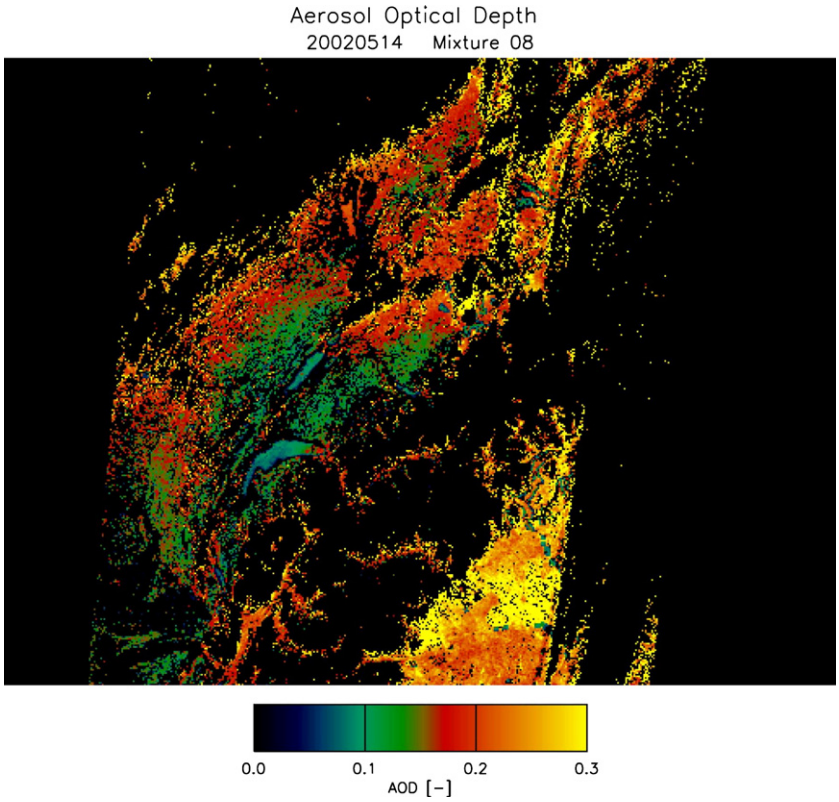

Fig. 15. Aerosol optical depth AOD (550 nm) map derived with the simultaneous retrieval method for May 14, 2002 (low aerosol case). Note the scale difference between Figs. 15 and 16. See Fig. 4 for radiance map and topography.

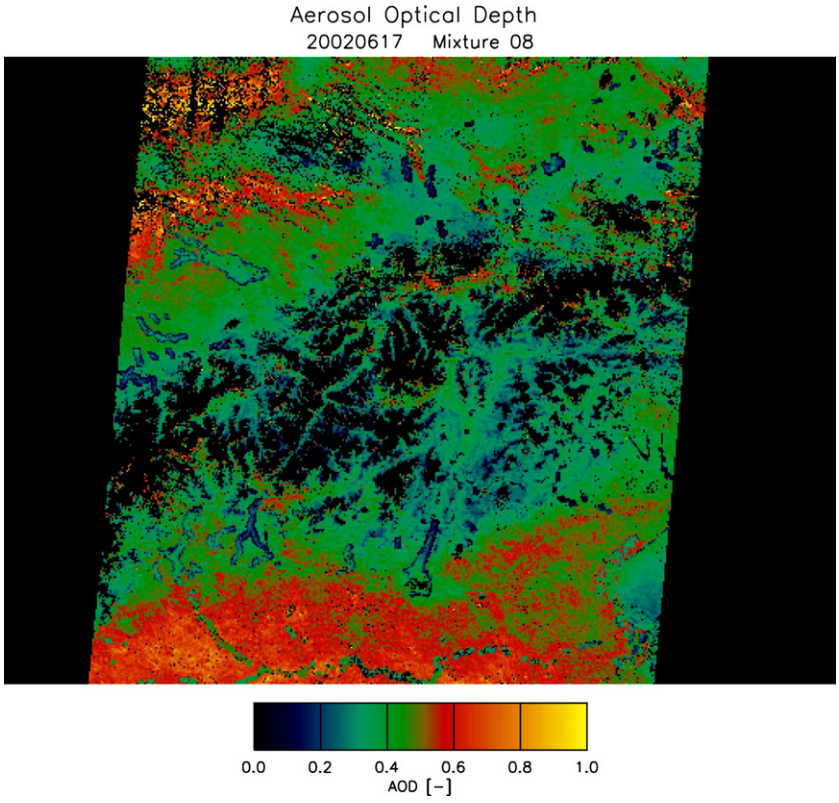

Fig. 16. Aerosol optical depth AOD (550 nm) map derived with the simultaneous retrieval method for June 17, 2002 (high aerosol case). Note the scale difference between Figs. 15 and 16. See Fig. 5 for radiance map and topography.

Close to the sun photometer station at Payerne, most of the ($\beta_{e,in}$ (550 nm), $\rho_{surf,in}$) intersections are located at negative extinction coefficients. The retrieved value of $\overline{\beta_e}$ (550 nm) would amount to -0.067 km^{-1} if positive and negative intersections were considered in the retrieval. The difference between the values over Lake Neuchatel and over Payerne is about 0.1 km^{-1}, which is in good agreement with the corresponding difference found for Ispra. Based on this result we suppose that this value is applicable as a first guess to other vegetation sites to match $\overline{\beta_e}$ (550 nm) and $\overline{\mathrm{AOD}}$ (550 nm) over water and over vegetation.

4.2.4. AOD maps

Maps of AOD (550 nm) generated with the simultaneous retrieval method are displayed in Figs. 15 (May 14, 2002) and 16 (June 17, 2002). We used land masks provided by the MISR Ancillary Geographic Product (AGP) to separate water and land subregions. Lambertian surfaces were assumed for water. Land surfaces were parameterized with the BRF parameters derived for agriculture. Prior to the calculation of the AOD we increased the $\overline{\beta_e}$ (550 nm) retrieved over land by a constant difference between water and vegetation values as explained in the previous section. A spatially independent difference of 0.1 km^{-1} and 0.2 km^{-1} was set for May 14 and for June 17, respectively. Snow covered subregions are rejected if ρ_{surf} (671 nm)>0.2. Clouds are disregarded by the same threshold or by an excessive scatter of the characteristic functions intersections. Subregions with missing data or with AOD uncertainties larger than 0.02 (for May 14) and 0.06 (for June 17) were set to 0.

AOD values north of the Alps are generally lower than in the Po basin on both days. Increased aerosol loads are also found in the valley bottoms. Thin clouds and contrails, which appear as high aerosol concentrations, are detected on June 17 in the north of the scene as well. The spatial features are similar to those of the MISR aerosol product (Figs. 6 and 7).

5. Discussion and conclusions

A novel algorithm was developed to retrieve simultaneously aerosol and surface optical properties. This method is based on so called characteristic functions $\rho_{surf}=f_{\lambda,cam}$ (β_e (550 nm)), which are generated with simulated and measured radiances. β_e (550 nm) and ρ_{surf} are the ground level aerosol extinction coefficient at 550 nm and the surface reflectance, respectively. For undisturbed atmospheric conditions over lake water the intersections of the characteristic functions calculated with the radiances of all cameras of a given spectral band form a cluster. It is possible to derive an average ground level aerosol extinction coefficient $\overline{\beta_{e,\lambda}}$ (550 nm) for each band using the respective MISR radiance data of those bands. In theory, these 4 values are equal if the atmospheric and the aerosol conditions are the same in the model as in reality. If a different, unrealistic mixture is used in the simulations, the intersections still cluster, but the most likely values $\overline{\beta_{e,\lambda}}$ (550 nm) are no longer wavelength independent. The best-fit extinction coefficient $\overline{\beta_e}$ (550 nm) is obtained for that mixture (the optimum mixture), for which the scatter of the most likely values $\overline{\beta_e}$ (550 nm) retrieved for the 4 bands is minimal. For these conditions best-fit values $\overline{\beta_e}$ (550 nm) and $\overline{\mathrm{AOD}}$ (550 nm) can be estimated as weighted averages of $\overline{\beta_{e,\lambda}}$ (550 nm) and AOD over the spectral bands, the weights being the inverse squares of the respective uncertainties.

We tested the simultaneous retrieval algorithm for Lago Maggiore close to the sun photometer station Ispra in northern Italy. On June 17, 2002, a day with relatively high aerosol load, $\overline{\mathrm{AOD}}$ (550 nm)$=0.355\pm0.011$ was obtained, which is in fairly good agreement with the sun photometer measurement (0.42 ± 0.01) and the corresponding value of the MISR aerosol product (0.386 ± 0.102). A similar agreement is observed for May 14, 2002, which was characterized by a relatively low aerosol load. Over vegetation, however, the retrieved AODs are significantly lower than those obtained over water. For those targets, the BRFs used in MODTRAN 4 were approximated by the Ross–Li approach with parameters that reproduce the BRFs for the 9 cameras provided by the MISR surface product best.

We conclude that the simultaneous retrieval algorithm has the potential of providing realistic aerosol properties over Lambertian water targets on a spatial resolution of 1.1 km., thus enhancing the resolution of the MISR aerosol product (17.6 km). For land targets, however, the radiance look-up tables must be improved. After having tested numerous parameter variations without obtaining any reasonable best-fit extinction coefficients and AODs over vegetation, we believe that the full coupling of BRF and DISORT, which is not yet implemented in the current MODTRAN 4 version, has the potential of yielding better results. The extinction coefficients over vegetation that are based on simulations of an improved version are expected to be greater than the current values. On the basis of $\overline{\beta_e}$ (550 nm) retrievals over water and over vegetation targets located close to each other, differences of 0.1 km^{-1} and 0.2 km^{-1} were estimated for May 14 and June 17, respectively. Finally, the retrieval algorithm has to be validated based on a larger number of days and a greater extension of the test domain.

Acknowledgements

This project was financially supported by the Federal Office for the Environment, FOEN (Bundesamt fuer Umwelt, BAFU).

We wish to thank Ralph Kahn and John Martonchik from the Jet Propulsion Laboratory (JPL) for the fruitful discussions. The first author is grateful to Chris Borel and Sig Gerstl for their hospitality and assistance during his stay at the Los Alamos National Laboratory (LANL). MISR data were obtained from the NASA Langley Research Center Atmospheric Sciences Data Center. We acknowledge the courtesy of Laurent Vuilleumier and Stephan Nyeki (MeteoSchweiz) for providing the IAP/CHARM sun photometer data, on which MeteoSchweiz hold full copyright. We thank Giuseppe Zibordi (JRC Ispra) for giving access to the sun photometry from the Ispra AERONET site and Lex Berk from Spectral Sciences Inc. for the information exchange and assistance regarding MODTRAN 4 issues.

References

Acharya, P. K., Berk, A., Anderson, G. P., Larsen, N. F., Tsay, S. -C., & Stamnes, K. H. (1999). MODTRAN4: Multiple scattering and Bi-directional Reflectance Distribution Function (BRDF) upgrades to MODTRAN. *SPIE Proceeding on Optical Spectroscopic Techniques and Instrumentation for Atmospheric and Space Research III*, *vol. 3756*. (pp. 354−362).

Berk A. (2005), personal communication.

Berk, A., Anderson, G. P., Acharya, P. K., Hoke, M. L., Chetwynd, J. H., Bernstein, L. S., et al. (2003). MODTRAN4 version 3 revision 1 user's manual. *Air Force Research Laboratory, Space Vehicles Directoriate, Air Force Materiel Command, Hanscom AFB, MA 01731-3010, Hanscom*.

Berk, A., Anderson, G. P., Bernstein, L. S., Acharya, P. K., Dothe, H., Matthew, M. W., et al. (1999). MODTRAN4 radiative transfer modeling for atmospheric correction. *SPIE Proceeding on Optical Spectroscopic Techniques and Instrumentation for Atmospheric and Space Research III*, *vol. 3756*. (pp. 348−353).

Cox, C., & Munk, W. (1955). Some problems in optical oceanography. *Journal of Marine Research*, *14*, 63−78.

Diner, D. J., Beckert, J. C., Reilly, T. H., Bruegge, C. J., Conel, J. E., Kahn, R., et al. (1998). Multiangle Imaging SpectroRadiometer (MISR) description and experiment overview. *IEEE Transactions on Geoscience and Remote Sensing*, *36*(4), 1072−1087.

Dockery, D. W., Pope, A. C., Xu, X., Spengler, J. D., Ware, J. H., Fay, M. E., et al. (1993). An association between air pollution and mortality in six U.S. cities. *New England Journal of Medicine*, *329*, 1753−1759.

EOSDIS (2001). Earth observing system data gateway. http://redhook.gsfc.nasa.gov/~imswww/pub/imswelcome/

Fischer, P. H., Brunekreef, B., & Lebret, E. (2004). Air pollution related deaths during the 2003 heat wave in The Netherlands. *Atmospheric Environment*, *38*(8), 1083−1085.

Holben, B. N., Eck, T. F., Slutsker, I., Tanre, D., Buis, J. P., Setzer, A., et al. (1998). AERONET— A federated instrument network and data archive for aerosol characterization. *Remote Sensing of Environment*, *66*(1), 1−16.

Houghton, J. T., Ding, Y., Griggs, D. J., Noguer, M., van der Linden, P. J., & Xiaosu, D. E. (2001). *Climate change 2001: The scientific basis. Contribution of working group I to the third assessment. Report of the Intergovernmental Panel on Climate Change (IPCC).* Cambridge: Cambridge University Press.

Kahn R. (2006), personal communication.

King, M. D., Kaufman, Y. J., Tanre, D., & Nakajima, T. (1999). Remote sensing of tropospheric aerosols from space: Past present, and future. *Bulletin of the American Meteorological Society*, *80*(11), 2229−2254.

Lewicki, S., Moroney, C., Crean, K., Gluck, S., Miller, K., & Paradise, S. (2003). *MISR data products specifications.* JPL D-13963, Revision H, JPL.

Lucht, W., Schaaf, C. B., & Strahler, A. H. (2000). An algorithm for the retrieval of albedo from space using semiempirical BRDF models. *IEEE Transactions on Geoscience and Remote Sensing*, *38*(2), 977−998.

Martonchik, J. V., & Bruegge, C. J. (2000). A review of reflectance nomenclature used in remote sensing. *Remote Sensing Reviews*, *19*, 9−20.

Martonchik, J. V., Diner, D. J., Kahn, R. A., Ackerman, T. P., Verstraete, M. M., Pinty, B., et al. (1998). Techniques for the retrieval of aerosol properties over land and ocean using multiangle imaging. *IEEE Transactions on Geoscience and Remote Sensing*, *36*(4), 1212−1227.

NASA/ASDC (2002). Langley ASDC–MISR data sets. http://eosweb.larc.nasa.gov/PRODOCS/misr/table_misr.html

NASA_Langley_ASDC (2006). MISR order and customization tool. http://l0dus01u.ecs.nasa.gov/cgi-bin/MISR_ordtool/main.cgi

Nicodemus, F. E., Richmond, J. C., Hsia, J. J., Ginsberg, I. W., & Limperis, T. (1977). *Geometrical considerations and nomenclature for reflectance.* Washington: National Bureau of Standards NBS MN-160.

Nyeki, S., Eleftheriadis, K., Baltensperger, U., Colbeck, I., Fiebig, M., Fix, A., et al. (2002). Airborne lidar and in-situ aerosol observations of an elevated layer, Leeward of the European Alps and Apennines. *Geophysical Research Letters*, *29*(17), 1852. doi:10.1029/2002GL014897

Rahman, H., Pinty, B., & Verstraete, M. M. (1993). Coupled surface-atmosphere reflectance (Csar) model.2. Semiempirical Surface model usable with Noaa advanced very high-resolution radiometer data. *Journal of Geophysical Research-Atmospheres*, *98*(D11), 20791−20801.

Stedman, J. R. (2004). The predicted number of air pollution related deaths in the UK during the August 2003 heatwave. *Atmospheric Environment*, *38*(8), 1087−1090.

Wagner T., Burrows J., Deutschmann T., Dix B., Hendrick F., von Friedeburg C., Frieß U., et al. (in press). Comparison of box-air-mass-factors and radiances for MAX-DOAS-geometries calculated from different UV/visible radiative transfer models. *Atmospheric Chemistry and Physics.*

Wanner, W., Li, X., & Strahler, A. H. (1995). On the derivation of kernels for kernel-driven models of bidirectional reflectance. *Journal of Geophysical Research*, *100*(10/2), 21077−21090.

Wanner, W., Strahler, A. H., Hu, B., Lewis, P., Muller, J. P., Li, X., et al. (1997). Global retrieval of bidirectional reflectance and albedo over land from EOS MODIS and MISR data: Theory and algorithm. *Journal of Geophysical Research-Atmospheres*, *102*(D14), 17143−17161.